Chemical Geology 635 (2023) 121619

Contents lists available at ScienceDirect

Chemical Geology

journal homepage: www.elsevier.com/locate/chemgeo

Early diagenetic mobilization of rare earth elements and implications for the Ce anomaly as a redox proxy

Kun Zhang *, Graham A. Shields

Department of Earth Sciences, University College London, WC1E 6BT, UK

ARTICLE INFO

Editor: Karen Johannesson

Keywords:
Rare earth elements
Ce anomaly
Early diagenesis
Sequential leaching
Redox proxy

ABSTRACT

The Rare Earth Elements (REE) archived in carbonate rocks retain a wealth of information on paleo-seawater chemistry and local-regional redox conditions. However, interpretations are often ambiguous due to the potential for REE remobilization in marine environments. In this regard, many carbonate rocks that retain primary seawater isotopic signatures exhibit non-seawater-like REE patterns, implying either unusual REE behaviour in seawater or diagenetic overprinting of otherwise well-preserved rock samples. Here, we apply sequential leaching to constrain the possible effects of different REE-bearing phases on measured carbonate REE patterns in order to address this quandary. Our results show that the exchangeable phase contains negligible REE, but could be an important host phase for other elements such as Sr, Ba and K. The acidified hydroxylamine hydrochloride leach is shown here not only to dissolve Fe–Mn oxides but also phosphate minerals, which induces middle REE enrichment in corresponding leachates of dolostone samples in our study. The demonstrable Fe–Mn oxide phase in limestone samples is characterized by middle and/or light REE enrichment and positive Eu anomalies, which are attributed to hydrothermal processes and continuing exchange with marine fluids after initial precipitation. The non-seawater-like REE patterns observed in the carbonate phase of otherwise well-preserved limestones resemble those of the co-existing Fe–Mn oxide fraction, and are interpreted to reflect the dissolution of REE carrier phases during early diagenesis. This view is supported by fluid-rock interaction modelling, which shows how REE can be mobilized at relatively low fluid/rock ratios in shallow porewaters. Non-seawater-like REE patterns may therefore be caused by the incorporation of REE from shallow porewaters before final lithification due to an elevated flux of particulate REE carrier phases, e.g. Fe–Mn oxides and organic matter, to the seafloor. In spite of the sensitivity of carbonate REE patterns to early diagenetic exchange, the co-occurrence of non-seawater-like patterns with primary strontium and carbon isotope values suggests that REE should not be viewed as a general indicator for the preservation of other geochemical proxies. Importantly, Ce anomalies of the carbonate phase will also be affected by porewaters, masking primary seawater values. Our results favour a reevaluation of redox interpretations by taking into account REE patterns as a whole.

1. Introduction

The Rare Earth Elements (REE), as defined by the International Union of Pure and Applied Chemistry (IUPAC), include fifteen lanthanides plus yttrium and scandium (Connelly et al., 2005). Geochemists commonly consider yttrium alongside the lanthanides in normalised 'spider' diagrams, in which both are normalised against shale, e.g. post-Archean Australian Shale (PAAS). In order to discriminate from earlier studies that rarely reported Y data, spider plots are sometimes referred to as REY (or REE + Y) patterns (rare earth elements plus yttrium; e.g. Kamber and Webb, 2001; Bau et al., 2014; Tostevin et al., 2016a). The similar electronic configurations yet gradually decreasing ionic radii across the REE series enable them to behave coherently, while exhibiting generally modest but systematic fractionation in the surface environment, making the REE particularly useful for tracing natural processes. In modern oceans, heavy REE (HREE) are preferentially complexed with carbonate ions while light REE (LREE) are preferentially adsorbed onto particle surfaces, leading to relative HREE enrichment in seawater (Elderfield and Greaves, 1982; Byrne and Kim, 1990; Sholkovitz et al., 1994; Schijf et al., 2015). The greater surface complexation stabilities of Ho relative to Y also give rise to the superchondritic Y/Ho ratios of seawater, despite their similar ionic radii (Nozaki et al., 1997). Cerium

* Corresponding author.
E-mail addresses: ucfbkzh@ucl.ac.uk (K. Zhang), g.shields@ucl.ac.uk (G.A. Shields).

https://doi.org/10.1016/j.chemgeo.2023.121619
Received 2 March 2023; Received in revised form 27 June 2023; Accepted 28 June 2023
Available online 30 June 2023

(III) is unique among the REE in that it is readily oxidized to relatively insoluble Ce(IV), resulting in relative Ce depletion (a negative Ce anomaly) in oxic seawater (De Baar et al., 1985; Sholkovitz et al., 1994; Ohta and Kawabe, 2001). Due to the rapid scavenging of REE by particles, the ocean residence time of REE is estimated at about 10^2–10^3 yrs. (Alibo and Nozaki, 1999). Consequently, REE patterns and Ce anomalies are indicative of local processes only.

The REE patterns in rocks are controlled by the fluid characteristics and fractionation processes during and/or after deposition. It has been demonstrated that chemical sedimentary rocks, including carbonate rocks, can preserve seawater REE patterns without significant fractionation (Webb and Kamber, 2000; Nothdurft et al., 2004). Therefore, REE patterns, and especially Ce anomalies, in carbonate rocks are commonly applied to infer seawater redox conditions in deep time (e.g. Ling et al., 2013; Tostevin et al., 2016b; Wallace et al., 2017; Liu et al., 2021). The seawater-like REE patterns found in carbonate rocks of varying ages lend further support that they can be a reliable and useful proxy to understand ancient seawater chemistry (Zhang and Shields, 2022). Given their importance in paleoenvironment reconstruction, some attempts have been made to develop robust sequential leaching methods with the aim of retrieving primary REE patterns in carbonate rocks without attacking non-carbonate phases (e.g. Zhang et al., 2015; Tostevin et al., 2016a; Cao et al., 2020). This is because non-carbonate phases, such as silicates, Fe–Mn oxides, phosphates and organic matter, have higher REE concentrations and distinct patterns, potentially complicating the interpretation of measured REE patterns and Ce anomalies. It has been shown that weak acid leaching and partial dissolution hold the greatest promise for extracting primary REE patterns (e.g. Cao et al., 2020). However, whether leaching methods based on relatively pure carbonate rocks and manufactured impure limestones are applicable to natural impure carbonate rocks remains unclear. Furthermore, while several studies have focused on sequentially leached carbonate phases (Zhang et al., 2015; Tostevin et al., 2016a), little attention has been paid to non-carbonate phases in carbonate rocks, leaving open the question of their influence on measured carbonate REE patterns.

The interpretation of REE patterns and Ce anomalies in carbonate rocks also bears heavily on our understanding of REE behaviour during diagenesis. Although it is broadly accepted that carbonate REE patterns are resistant to diagenetic alteration, non-seawater-like REE patterns are not uncommon in carbonate rocks, even when processed using proven leaching methods (e.g. Zhang et al., 2018; Ward et al., 2019). Some researchers have proposed that these anomalous REE patterns (e.g. MREE enrichment) may indeed reflect primary seawater characteristics (e.g. Lécuyer et al., 2004; Emsbo et al., 2015; Hood and Wallace, 2015), and yet such patterns have not been found in modern oceans. In addition, with increasing amounts of high-quality data, it is becoming clear that non-seawater-like REE patterns are frequently observed in carbonate rocks characterized by globally correlative carbon isotope excursions, especially for rocks of Neoproterozoic age (Ward et al., 2019; Zhao et al., 2021). If we accept that carbon isotope values represent primary or near primary ocean composition, at least locally, it is difficult to reconcile these two proxies as both are thought to be relatively resistant against diagenetic alteration (e.g. Banner et al., 1988; Lau and Hardisty, 2022). On the other hand, German and Elderfield (1990) proposed that only sediments undergoing oxic diagenesis preserve truly seawater REE signatures, while carbonate rocks commonly form from metastable precursors, in which case both carbon isotopes and REE patterns seem likely to reflect porewater chemistry. Such an unresolved conundrum implies that there might be some gaps in our understanding of REE cycling in Earth's surface environment that could potentially hamper interpretations of local redox conditions during critical intervals.

Here we attempt to shed light on some of these issues by applying sequential leaching to carbonate rocks of different purities. We demonstrate that different operationally-defined phases exhibit distinctive REE patterns, while non-carbonate phases can retain a significant proportion of the total REE content of impure carbonate rocks. Considering these phase partitioning experiments, observations of modern porewater REE and fluid-rock modelling, we show how carbonate REE patterns can be modified during early diagenesis, thereby providing a potential resolution to reconcile the conundrum of primary $\delta^{13}C$ excursions (and potentially other geochemical proxies) with non-seawater-like REE patterns.

2. Materials and methods

2.1. Samples

Twenty carbonate rock samples containing a wide range of carbonate contents and TOC values were selected for phase partitioning experiments, ten of which were collected from Member III of the Gaoyuzhuang Formation (hereafter referred to as GYZ) at Gan'gou section in North China that was deposited at about 1.6 Ga in a subtidal environment (Tang et al., 2016). The GYZ samples selected here span a previously revealed negative carbon isotope excursion (Zhang et al., 2018), and comprise impure organic-rich carbonate rocks (mainly dolostones) with relatively low carbonate (averaging 54%) and relatively high TOC contents (averaging 1.34%). The other ten carbonate rock samples were collected from the Taishir Formation of the Tsagaan-Olom Group at Tsagaan Gol in western Mongolia that were deposited between the Sturtian and Marinoan 'Snowball' glaciations of the Cryogenian Period. The Taishir Formation is subdivided into four members (T1-T4) and is proposed to represent deposition in a mid- to outer-ramp environment, i.e. below fair-weather wave base (Bold et al., 2016). The studied Taishir samples, mainly from the T1 and T2 members, comprise relatively pure limestones (carbonate content ~95%) with low TOC contents (averaging 0.32%). Detailed description of the samples can be found in Shields et al. (2002). The carbonate samples (GYZ and Taishir) were crushed into small rock chips with clean chips further ground into fine powders using an agate TEMA mill.

Two certificated reference materials BCS-CRM 393 and NBS-SRM 1c were digested following the same sequential leaching scheme. CRM 393 is a pure limestone, which contains 55.4% CaO and 0.15% MgO with Fe_2O_3, MnO, and Al_2O_3 contents of 0.005%, 0.001%, and 0.01%, respectively. SRM 1c is an argillaceous limestone containing 50.3% CaO and 0.42% MgO with comparatively higher Fe_2O_3, MnO, and Al_2O_3 contents of 0.55%, 0.025%, and 1.30%, respectively.

2.2. Sequential leaching protocol

Systematic studies on sequential leaching of carbonate-bound REE from carbonate rocks generally suggest that partial carbonate dissolution with weak acids can minimize non-carbonate contamination (e.g. Fe–Mn oxides, clay, phosphate and organic matter; Rongemaille et al., 2011; Zhang et al., 2015; Tostevin et al., 2016a; Cao et al., 2020). However, it remains unclear whether existing leaching protocols are applicable to natural impure carbonate rocks. The REE patterns of non-carbonate phases in carbonate rocks are also rarely investigated specifically, hindering our understanding of their potential influence on measured carbonate REE patterns. Here, a six-step sequential leaching scheme was designed to separate different REE phases in carbonate rocks (Table 1).

For each sample, ~500 mg powder was weighed into acid cleaned 50 ml polypropylene tubes. In the first step, 20 ml of 1 M ammonium acetate (pH 6.9) was added to the sample tubes that were then placed in an ultrasonic bath for 0.5 h. A certain amount of 0.3 M acetic acid was added to the tubes in the second step to partially dissolve carbonates, while excess 0.3 M acetic acid was invoked in the third step with the aim of dissolving all remaining carbonates. The ultrasonication time was set at 0.5 h and 4 h, respectively, for the second and third steps. In the fourth and fifth steps, 40 ml 0.1 M hydroxylamine hydrochloride in 25% (v/v) acetic acid (pH 1.6) was added to the tubes. This was designed to avoid

Table 1
Reagents used in phase partitioning experiments and respective target phases.

	Target phases	Ultrasonication	Taishir samples	GYZ samples and reference materials
Fraction 1	Exchangeable	0.5 h	1 M ammonium acetate	1 M ammonium acetate
Fraction 2	Carbonate	0.5 h	0.3 M acetic acid	0.3 M acetic acid
Fraction 3	Carbonate	4 h	0.3 M acetic acid	0.3 M acetic acid
Fraction 4	Fe–Mn oxide	6 h	0.1 M NH_2OH HCl in 25% acetic acid	0.1 M NH_2OH HCl in 25% acetic acid
Fraction 5	Fe–Mn oxide	6 h	0.1 M NH_2OH HCl in 25% acetic acid	0.1 M NH_2OH HCl in 25% acetic acid
Fraction 6	Organic matter/silicate	–	–	10% HNO_3 after ashing

excess acidified reagent, which could attack the silicate fraction. An additional leaching step ensured complete Fe–Mn oxide dissolution prior to extracting the organic matter/silicate phase. The tubes were ultrasonicated in the water bath at room temperature for 6 h, during which the tubes were shaken by hand after every 1 h. To our knowledge, this is the first time that this reagent has been applied to ancient carbonate rocks, although an alternative reducing reagent, i.e. hydrous hydrazine and ammonium citrate in ammonium hydroxide, has been applied to Cretaceous limestones (Clarkson et al., 2020). The residues from the fifth step were transferred to crucibles, ground and ashed in a furnace at 550 °C for 3 h, before being dissolved in 5 ml 10% HNO_3. The supernatants of each leaching step were obtained by centrifugation at 4500 rpm for 5–10 min. The supernatants were then filtered into acid cleaned Teflon beakers using 0.22 μm syringe filters, dried on a hot plate and re-dissolved in 2% HNO_3. Concentrated nitric acid was added to the dried supernatants of the fourth and fifth steps before re-dissolution in 2% HNO_3 to eliminate excess reducing agent (Chester and Hughes, 1967). The residues after each leaching step were rinsed with de-ionised water (18.2 MΩ) three times and then dried completely in an oven in order to determine the weight loss at each step. The target phases thought to be extracted by each sequential leaching step are listed in Table 1.

2.3. Elemental analysis

All leachates were diluted in 2% HNO_3 for major and minor element analysis (Ca, Mg, Fe, Mn, Al, P, Sr, Ba, K) using a Varian 720 inductively coupled plasma optical emission spectrometer (ICP-OES) at University College London. Phosphorus analysis was aided with the polyboost function (i.e., argon purging; Hayakawa et al., 1982). Standard solutions were run after every ten samples to monitor the long-term drift, which gave a relative standard deviation of <3%. The precision was monitored by repeated analyses of two in-house bulk digested standards of SRM 88a (dolomitic limestone) and SGR-1 (Green River shale), and was typically better than 3% (supplementary material). The internal reproducibility determined by analyses of duplicate samples that underwent the same full procedure was generally better than 10%. Analyses of two rock standards agree with certified values within the error of uncertainty (see supplementary material for details).

For trace element analysis (REE and U), the stock solutions were further diluted in 2% HNO_3 to contain ~50 ppm Ca based on the ICP-OES results, while the stock solutions with very low Ca were diluted 5 to 50 fold. A 2 ppb indium spike was added as an internal standard to monitor the instrumental drift and matrix effects. These diluted solutions were analysed in different batches on an Agilent 7900 inductively coupled plasma mass spectrometer (ICP-MS) at University College London. Before each batch analysis, oxide interference was monitored using the formation rate of Ce oxide and the formation of 2+ ions was monitored using Ba^{2+}. Calibration curves were produced from multi-elemental artificial standard solutions that contained similar Ca concentration to sample solutions. Standard solutions analysed after every six samples gave a long-term drift with a relative standard deviation of <10%. The precision determined by repeated analysis of TMDA-70 (Fortified water), SGR-1 (Green River shale), and GSR-12 (dolostone) was typically better than 5% (supplementary material), while the internal analytical precision has a larger relative standard deviation for the heavy REE and leachates from the first fraction due to their low concentrations. The analysis of duplicates that were processed through the full and identical procedure shows an overall internal reproducibility of 5%. The accuracy was determined by the measurement of TMDA-70 and SGR-1, which showed values that were generally consistent with certified values within uncertainty (supplementary material). Blanks generally showed negligible element concentrations below the detection limit. It should be noted that all element concentrations mentioned hereafter are reported relative to the weight loss at each step, which is considered to reflect element distribution in different fractions better, although this will inevitably introduce uncertainties due to weighing. The REE concentration data are normalised against PAAS (shown with subscript N; Mclennan, 1989), and different REE anomalies are calculated based on geometric extrapolation and/or interpolation (Lawrence et al., 2006), as follows: $Ce/Ce^* = Ce_N \times Nd_N / Pr_N^2$; $Eu/Eu^* = Eu_N / (Sm_N^2 \times Tb_N)^{1/3}$; $Nd/Nd^* = Nd_N / (Pr_N^2 \times Sm_N)^{1/3}$.

3. Results

3.1. Major, minor and trace elements

For relatively pure Taishir limestone samples (Fig. 1a), only a small proportion of Ca, Mg, Fe, Mn, Al and P was shown to be in the exchangeable fraction (fraction 1). Significant amounts of Sr (5.8 ± 0.6%; mean ± 1 s.d., weight percentage of total extracted), U (7.8 ± 1.6%), Ba (17.9 ± 6.3%) and K (53 ± 10.6%) were liberated in fraction 1. Almost all Ca was liberated in fractions 2 and 3, accompanied by Mg (61.2%), Mn (76.7%), Sr (83.2%), Ba (65.9%), U (50.8%), and a smaller proportion of Fe (28.5%), Al (30.0%), K (29.2%), and P (5.8%). Fraction 4 is dominated by Fe (59.6 ± 7.2%), P (88 ± 13.4%), Al (51.3 ± 11.2%), and a lesser proportion of Mg (36 ± 19.1%), Mn (19.3 ± 13.6%), and U (38.0 ± 15.6%). Fraction 5 contains Fe, Al, and Mn at 11.9 ± 5.8%, 16.3 ± 4.9%, and 0.9 ± 0.6%, respectively.

The reference materials and GYZ samples were subjected to six leaching steps (Fig. 1b-d). Similar to Taishir samples, a significant amount of Ba and K, and a certain amount of Sr and U were released in fraction 1 with only a small amount of dissolved Ca, Mg, Fe and Mn. While nearly all Ca, Mg and Sr, and a substantial amount of Mn and U were released from reference materials in fractions 2 and 3 (Fig. 1c, d), only ~40–60% of those elements were liberated from the impure GYZ carbonate rocks. Iron and P were mainly released from reference materials in fractions 4 and 5 (Fig. 1c, d), whereas 42.1 ± 21.7% of Fe was liberated from GYZ samples in fraction 6 (Fig. 1b). The majority of Al was released in fraction 6, accompanied by a large amount of K from SRM 1c (an argillaceous limestone) and impure GYZ carbonate rocks (Fig. 1b-d).

Despite the discrepancies in dissolved weight percentages of different elements in different fractions among samples, their elemental concentrations show relatively consistent trends during sequential leaching (Fig. 2). In general, Fe and Al concentrations show increasing trends, whereas Sr concentrations exhibit a broad decreasing trend through sequential leaching. Manganese concentrations show a broadly increasing trend in fractions 1 through 4, with most showing a decrease in fraction 5. Barium and K concentrations are abnormally high in

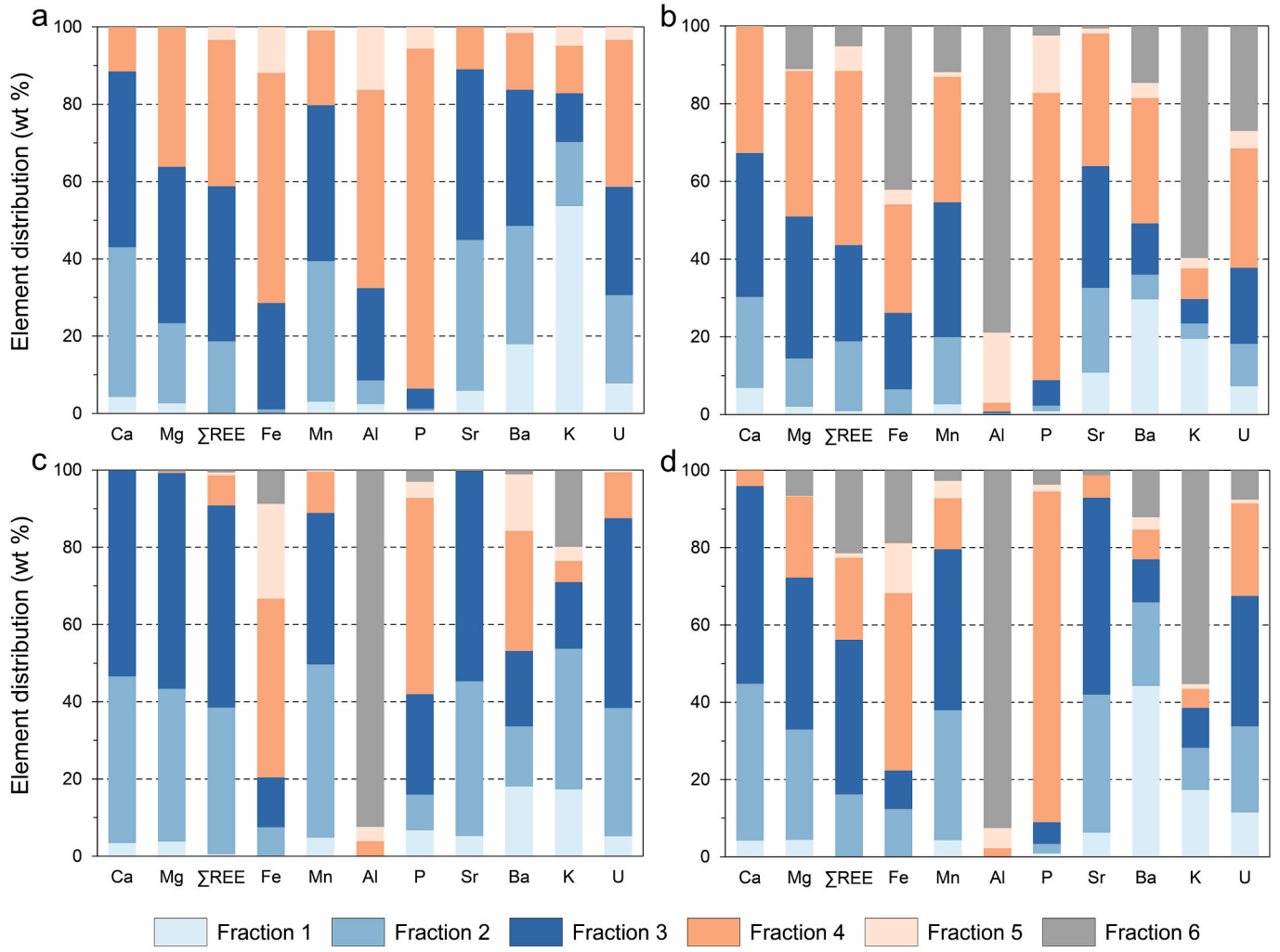

Fig. 1. Major, minor and trace element concentrations in different fractions, shown as weight percentage of total extracted. (a) Taishir samples, (b) GYZ samples, (c) CRM 393, (d) SRM 1c. Note that for (a) and (b), data represent averages of all Taishir and GYZ samples, respectively.

fraction 1, low in fractions 2 and 3, and gradually increase from fractions 4 to 6. Phosphorus and U concentrations are generally low in the first three fractions but increase significantly in fractions 4–6. It is also observed that the pure limestone (CRM 393) and argillaceous limestone (SRM 1c) have relatively low U concentrations in fraction 5.

3.2. Rare earth elements

Fraction 1 constitutes only a negligible part of total extracted REE in all samples (Figs. 1, 3). Fractions 2 and 3 contribute ~50–65% of total extracted REE in Taishir samples, ~40–50% in GYZ samples, ~85–90% in CRM 393, and ~40–75% in SRM 1c. Fraction 4 constitutes ~30–45% of the total extracted REE in Taishir samples, ~45% in GYZ samples, ~5–10% in CRM 393, and ~15–30% in SRM 1c. While fraction 5 and/or fraction 6 represent less than 5–12% of the total extracted REE in CRM 393, GYZ and Taishir samples, fraction 6 comprises more than 20% of the total extracted REE in SRM 1c (Figs. 1, 3).

The REE patterns in fraction 1 are characterized by pronounced positive Eu anomalies (see discussion in Section 4.1.1) and elevated Y/Ho ratios for CRM 393, SRM 1c and Taishir samples, whereas REE are characterized by MREE enrichment with an order of magnitude higher concentrations in impure GYZ carbonate rocks (Fig. 4–6). In fractions 2 and 3, CRM 393 and SRM 1c exhibit typically seawater-like REE patterns (Fig. 6). Taishir carbonate rocks show either slight MREE enrichment and/or seawater-like REE patterns, whereas GYZ carbonate rocks mainly exhibit relatively flat and/or MREE-enriched REE patterns (Figs. 4, 5). In fractions 4 and 5, nearly all samples exhibit LREE- and/or MREE-enriched patterns, although their concentrations can vary by more than an order of magnitude (Fig. 4–6). It is interesting to note that a seawater-like REE pattern with low REE content reappears in fraction 5 of CRM 393 (Fig. 6). In fraction 6, while CRM 393 and SRM 1c are characterized by significant LREE enrichment, GYZ carbonate rocks show relatively flat REE patterns (Figs. 5, 6).

In general, Y/Ho ratios gradually decrease while REE concentrations show a broadly increasing trend through the sequential leaching (Fig. 7). Pr_N/Yb_N and Sm_N/Yb_N ratios are lower whereas Dy_N/Sm_N ratios are generally higher in fractions 2 and 3 relative to fraction 4. It is noteworthy that the reference materials and GYZ samples exhibit opposing trends in these parameters between fractions 5 and 6. In addition, the Ce anomaly values of CRM 393 and SRM 1c are lower in fractions 2 and 3 than in the subsequent fractions, whereas the mean Ce anomaly values in Taishir and GYZ samples remain relatively stable from fraction 2.

4. Discussion

4.1. Phase partitioning

Sequential leaching can provide insights into the partitioning of elements among different phases of a bulk rock, but a perfect separation of different phases may not be achievable, due to incomplete dissolution,

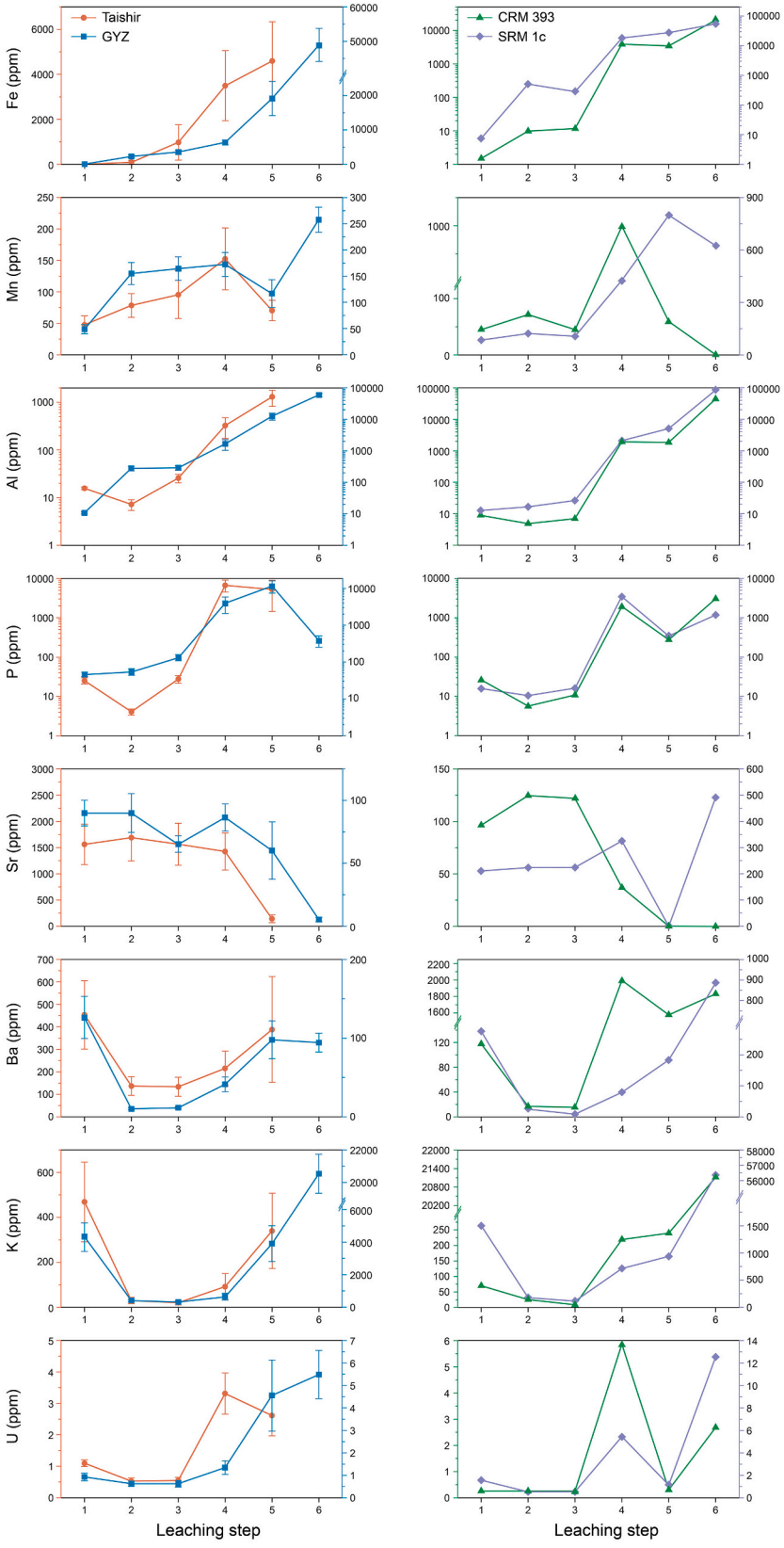

Fig. 2. Variation of major, minor and trace element concentrations across different leaching steps. Note that the data from the Taishir and GYZ samples are shown as mean values of all samples. Error bars represent ±1 SEM (standard error of the mean). For the plots on the left column, Taishir samples (circles) correspond to the scale on the left while GYZ samples (squares) correspond to the scale on the right. For the plots on the right column, CRM 393 (triangles) corresponds to the scale on the left while SRM 1c (diamonds) corresponds to the scale on the right.

simultaneous dissolution of different phases, and/or re-adsorption of elements (e.g. Sholkovitz, 1989; Filgueiras et al., 2002; Willis and Johannesson, 2011). Here, exchangeable, carbonate, Fe–Mn oxide and organic matter/silicate phases are operationally defined as corresponding to respective sequentially leached fractions (Table 1).

4.1.1. *Exchangeable phase*

The exchangeable phase includes metals weakly bound to the surface

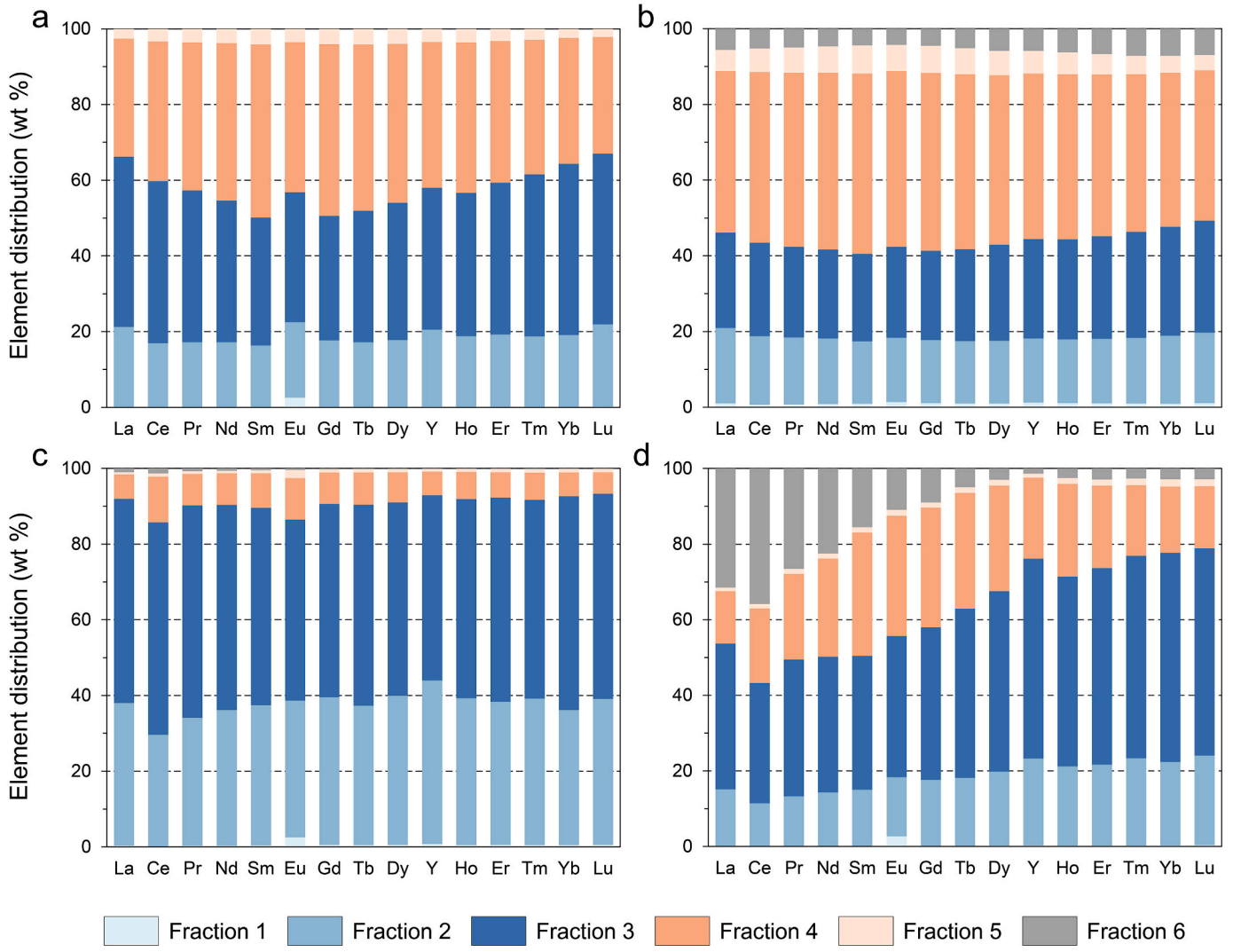

Fig. 3. Element distribution of rare earth elements in different fractions, shown as weight percentage of total extracted. (a) Taishir samples, (b) GYZ samples, (c) CRM 393, (d) SRM 1c. Note that for (a) and (b), data represent averages of all Taishir and GYZ samples, respectively.

of organic matter and clay minerals by weak electrostatic interaction (e.g. Tessier et al., 1979; Filgueiras et al., 2002; Willis and Johannesson, 2011). Previous studies have used dilute acetic (Zhang et al., 2015) and nitric acid (Tostevin et al., 2016a) to remove a certain percentage of carbonate before extracting lattice-bound REE from ancient carbonate rocks, which could have removed the exchangeable phase simultaneously. More recently, Cao et al. (2020) recommended 'cleaning' the samples with ammonium acetate. Ammonium ions can efficiently displace exchangeable REE bound to negatively charged surficial sites via ion-exchange (Moldoveanu and Papangelakis, 2012). However, it has also been demonstrated that ammonium acetate solution of even neutral pH (pH 7.0) may dissolve some carbonate possibly due to Ca-acetate complexation (Tessier et al., 1979; Bailey et al., 2000). Since the initial leachates of carbonates are commonly discarded (e.g. Zhang et al., 2015; Tostevin et al., 2016a), we adopt a neutral ammonium acetate (pH 6.9) solution to remove both exchangeable ions and a small amount of the carbonate fraction. Although ~3–7% Ca is consistently liberated in the exchangeable phase across these variable purity samples, the amount of REE released from GYZ samples is an order of magnitude higher (Fig. 7), indicating that a greater proportion of exchangeable REE occurs in impure carbonate rocks, due to the leaching of non-carbonate phases. Consistent with previous studies (e.g. Zhang et al., 2015; Lin et al., 2020), the exchangeable phase shows high concentrations of Ba, Sr and K in all samples, but intriguingly, the Al concentration is consistently low in the exchangeable phase possibly because of the neutral pH (e.g. Köhler et al., 2005). This suggests that a considerable amount of Ba, Sr and K (and potentially other trace elements) is related to the exchangeable phase but not to crystalline aluminosilicates. The commonly used detrital correction equation, which invokes Al to calculate authigenic trace element concentrations and isotope values (e.g. Bridgestock et al., 2018), may therefore cause unconstrained errors for those elements. In addition, it is well demonstrated that the exchangeable phase differs significantly from the carbonate phase in $^{87}Sr/^{86}Sr$, $\delta^{137/134}Ba$ and also $\delta^{98}Mo$ (e.g. Bailey et al., 2000; Li et al., 2011; Lin et al., 2020; Clarkson et al., 2020), and so it has been recommended to remove the exchangeable phase before leaching carbonates. Given that carbonate-bound trace metal isotopes are increasingly being applied to paleoenvironment studies and they may share the same issue, it is of critical importance to further hone leaching protocols for different metal isotope systems.

It may be surprising to find that the exchangeable REE patterns in relatively pure carbonate rocks share common features with modern seawater REE patterns, e.g. positive La anomaly, HREE enrichment and superchondritic Y/Ho ratio (Figs. 4, 6), whereas the impure GYZ carbonate rocks are characterized by MREE enrichment and the absence of any significant negative Ce anomaly (Fig. 5). It should be noted that the

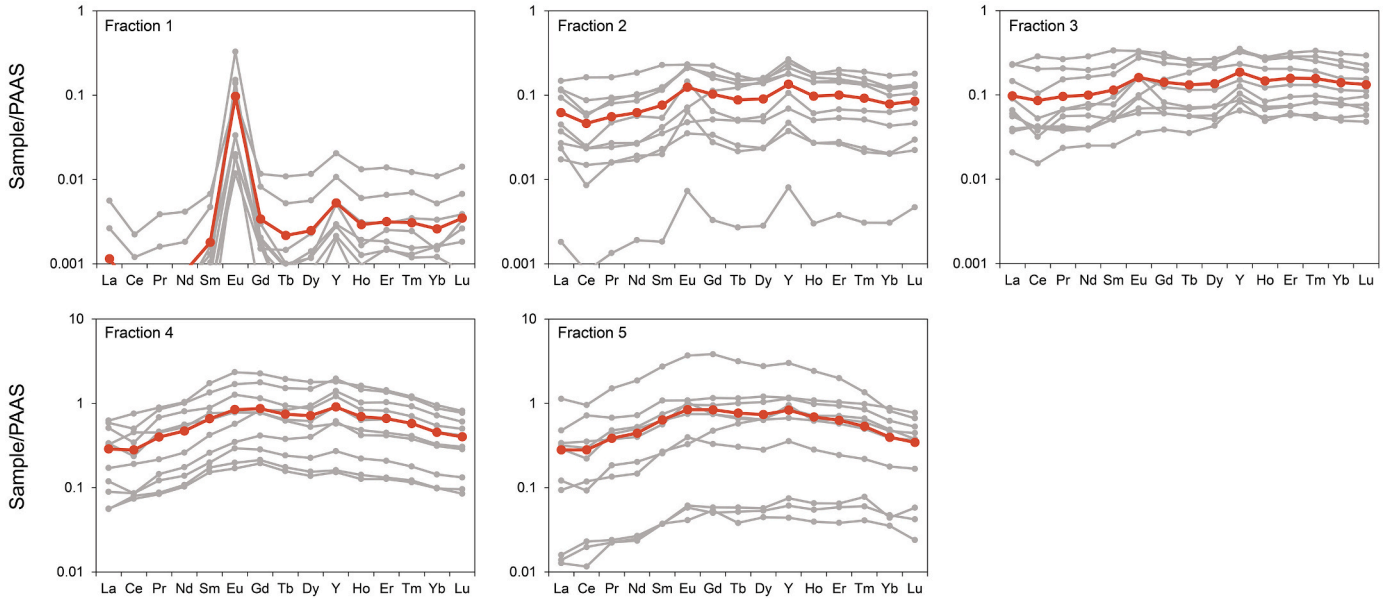

Fig. 4. Rare earth element patterns in relatively pure Taishir limestones from fractions 1–5. Ratios below 0.001 are not shown in the figure. Gray lines in each panel indicate REE patterns for each sample, and red lines represent average REE patterns of all samples. Note different vertical scales (normalised REE abundance) for fractions 1–3 versus fractions 4–5. (For interpretation of the references to colour in this figure legend, the reader is referred to the web version of this article.)

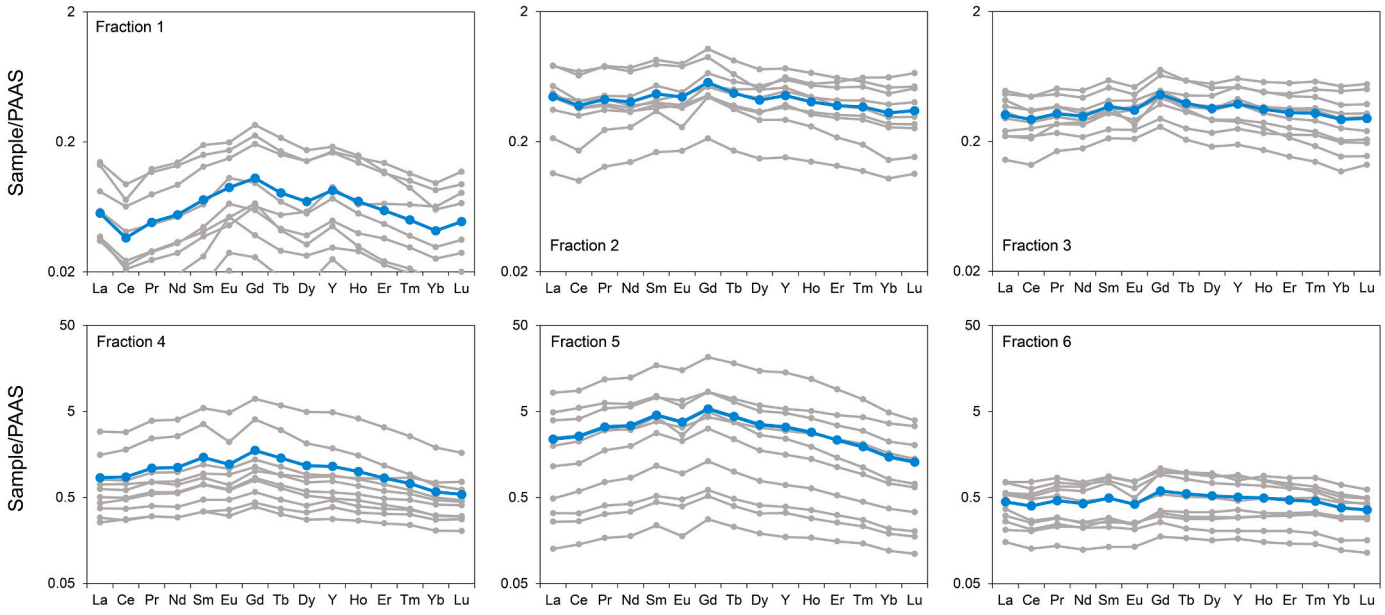

Fig. 5. Rare earth element patterns in relatively impure GYZ dolomitic carbonate rocks from fractions 1–6. Gray lines in each panel indicate REE patterns for each sample, and blue lines represent average REE patterns of all samples. Note different vertical scales (normalised REE abundance) for fractions 1–3 versus fractions 4–6. (For interpretation of the references to colour in this figure legend, the reader is referred to the web version of this article.)

REE concentrations of relatively pure carbonate rocks in fraction 1 are very low and near the detection limit, which is also consistent with previous studies (e.g. Phan et al., 2019; Cao et al., 2020). Therefore, these data should only be regarded as semi-quantitative or qualitative in some cases. By using ammonium acetate to extract exchangeable REE in Marcellus black and calcareous shales, Phan et al. (2019) also found seawater-like patterns but with HREE depletion, and this has been interpreted to result from the combined effects of diagenetic fluids that originated from evaporating seawater and the higher hydration energies of HREE causing less desorption. Instead, considering the typical seawater-like patterns (Figs. 4, 6) and given that small amounts of carbonates were also dissolved during ammonium acetate leaching (Fig. 1), we tentatively suggest that the REE patterns in fraction 1 reflect the combination of 'truly' exchangeable and carbonate-bound REE. The impure GYZ carbonate rocks contain relatively higher amounts of exchangeable REE (Fig. 7), and their REE patterns in fraction 1 consequently deviate from that in fraction 2 (Fig. 5). The relatively pure carbonate rocks, on the other hand, have negligible exchangeable REE and thus their REE patterns in fraction 1 are dominated by carbonate-bound REE, which is supported by the similarity between the REE patterns of fractions 1 and 2 (Figs. 4, 6).

The Ce anomalies in the exchangeable phase show considerable variability, and in some cases, even exhibit lower values than that of the carbonate phase (Fig. 7). However, it is important to emphasize the need

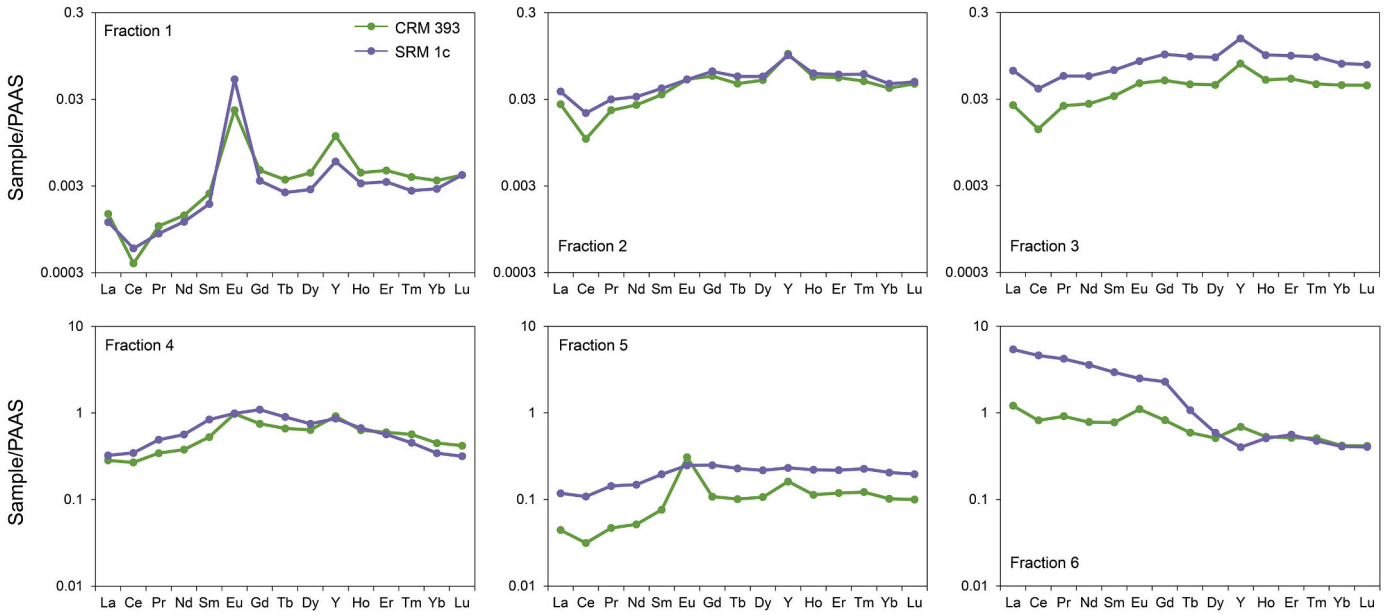

Fig. 6. Rare earth element patterns in CRM 393 (green lines) and SRM 1c (purple lines) from fractions 1–6. Note different vertical scales (normalised REE abundance) for fractions 1–3 versus fractions 4–6. (For interpretation of the references to colour in this figure legend, the reader is referred to the web version of this article.)

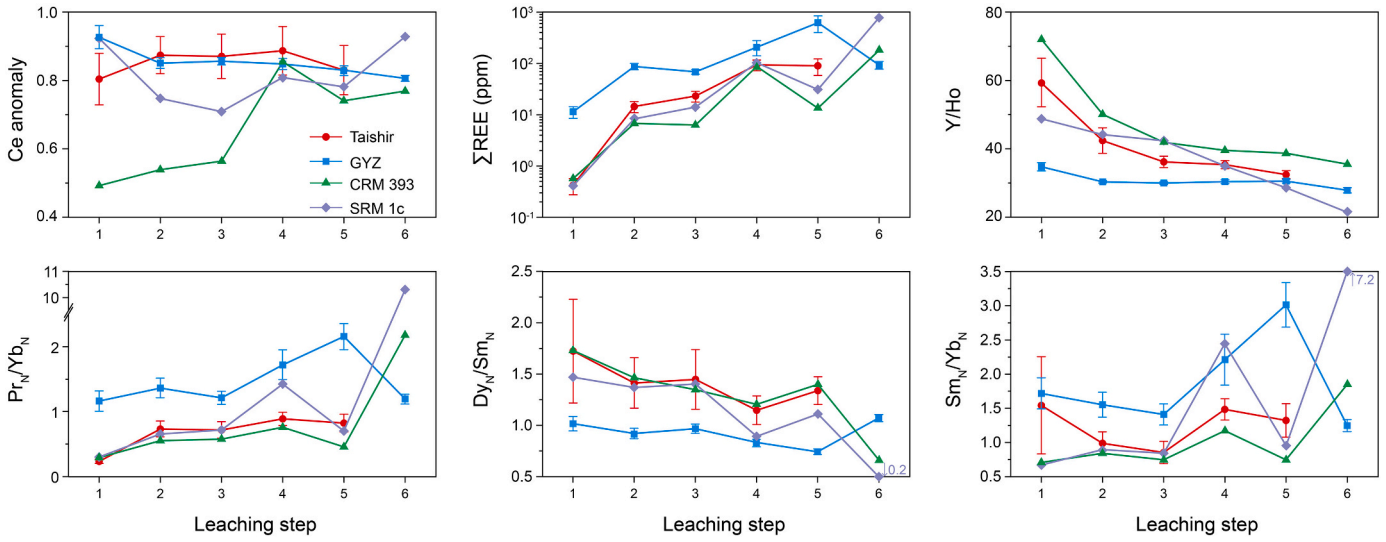

Fig. 7. Variation of REE parameters across different leaching steps. Note that the data from the Taishir (circles) and GYZ (squares) samples are shown as mean values of all samples. Error bars represent ±1 SEM.

for caution when interpreting Ce anomalies at such low REE concentrations. As shown in Fig. 8a, significant Ce anomalies, either negative or positive, are more likely to occur in samples with very low REE concentrations. Modern ICP-MS instrumentation may need to shift between analog and pulse count modes when measuring Ce in calibration standards and/or samples due to its relatively high concentration in marine sediments (Planavsky et al., 2010). The resulting calibration curve inevitably produces analytical uncertainties, which are further amplified at low concentrations (Wu et al., 2018). The Ce anomaly is also influenced by the precision of Pr and Nd since it is extrapolated from those two neighboring elements (Lawrence and Kamber, 2006), whereby Pr is more likely to be affected by analytical artefacts due to its generally lower concentration relative to Nd. A parameter referred to as a Nd anomaly has been introduced to constrain such issues (e.g. Bellefroid et al., 2018; Zhang and Shields, 2022), which should be around 1.0 in the case of conservative chemical behaviour and absence of analytical artefacts. Our samples with non-unity Nd anomalies tend to show a wide range in Ce anomalies (Fig. 8b). Therefore, we tentatively conclude that pronounced Ce anomalies in the exchangeable phase are likely to be analytical artefacts.

A most prominent feature of REE patterns in the exchangeable phase is the abnormally high Eu anomalies in relatively pure carbonate rocks (Figs. 4, 6) that have otherwise not been observed in chemical sedimentary rocks (e.g. Kato et al., 2006). Considering the low REE concentrations and contrastingly high Ba concentrations, the pronounced Eu anomalies are likely to have been caused by polyatomic interference from barium oxide produced during ICP-MS analysis (Dulski, 1994; Shields and Stille, 2001). This is supported by statistically robust covariation between Ba/Nd and Eu anomalies in our pure limestone samples as well as CRM 393 and SRM 1c (Fig. 9a). The Eu anomalies of

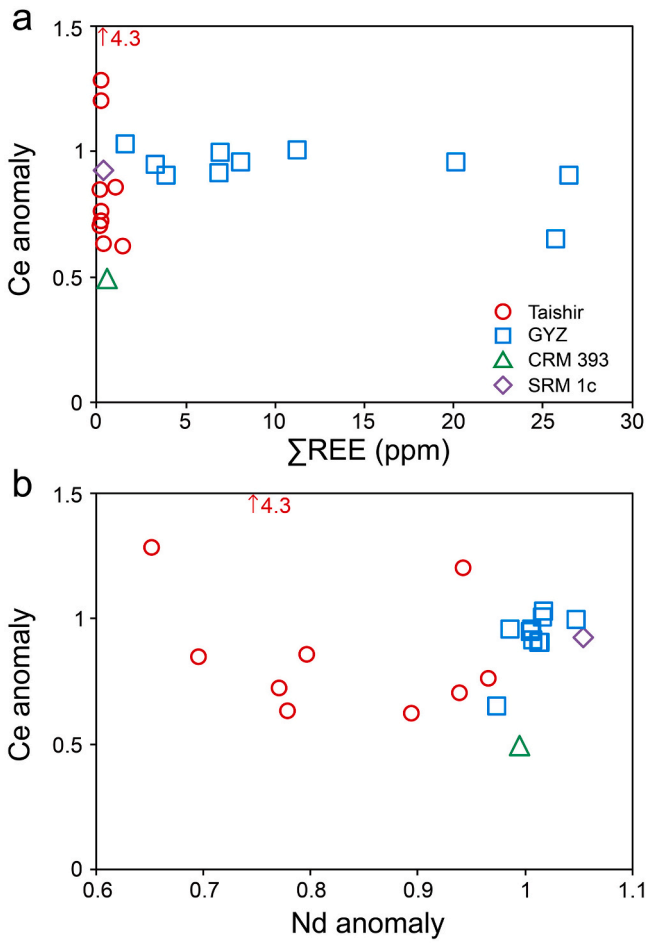

Fig. 8. Cross plots of Ce anomaly against (a) REE content and (b) Nd anomaly of the exchangeable phase in samples and reference materials.

GYZ samples, mostly around 1.0, also reveal good covariation with Ba/Nd (Fig. 9a), and those samples with relatively lower REE contents tend to exhibit higher Eu anomalies ($R^2 = 0.60$; not shown). Therefore, the apparent positive Eu anomalies in the exchangeable phase are most likely caused by barium compound interference during analysis.

The exchangeable phase also exhibits consistently the highest Y/Ho ratios among all sequentially leached fractions (Fig. 7). Although the ratios might be exaggerated to some extent because of the inherent uncertainty in measuring low Ho concentrations, the Y/Ho ratios are still the highest in the exchangeable phase of impure GYZ carbonate rocks (mean 34.7; Fig. 7), which have much higher REE concentrations and thus better analytical precision. This implies that the high Y/Ho ratio could be a primary feature of the exchangeable phase of carbonate rocks. Indeed, a high Y/Ho ratio has also been observed in the exchangeable phase of soils (e.g. SRM 2710; Mittermüller et al., 2016), Mn nodules and artificial, impure limestones (Cao et al., 2020). As discussed above, fraction 1 could contain the 'truly' exchangeable and carbonate-bound REE (Table 2), and its Y/Ho ratio should therefore reflect the combination of the two phases. Considering that fraction 1 has a consistently higher Y/Ho ratio than fraction 2 (carbonate phase), the 'truly' exchangeable phase should also have a higher Y/Ho ratio. One possible explanation is that the 'truly' exchangeable phase contains a higher content of Y relative to Ho, which is released into solution during ammonium acetate leaching. However, it is generally believed that compared with Y, Ho has a greater particle affinity due to a greater surface complexation stability (e.g. Nozaki et al., 1997; Bau et al., 1997). Nevertheless, ammonium acetate leaching may be only able to remove the ions attracted by weak electrostatic interactions, while not leaching relatively strongly complexed ions (Filgueiras et al., 2002; Moldoveanu and Papangelakis, 2012). The other possible explanation is that Y desorbs more efficiently relative to Ho during ammonium acetate leaching. Cation exchange is considered to be influenced by ionic potential and/or hydration energy or both (Moldoveanu and Papangelakis, 2012, 2016). The trivalent Y and Ho have similar ionic radii (~1.04 Å sixfold coordination; Shannon, 1976), and they also share similar hydration energies (~ −3640 kJ mol^{-1} in standard state; Rudolph and Irmer, 2015). The formation constant for Y complexation by single acetate is lower than that for Ho (Byrne and Liu, 1998). In addition, prolonged ammonium acetate leaching seems not to modify Y/Ho ratios significantly (Cao et al., 2020). Taken together, the high Y/Ho ratio of the 'truly' exchangeable phase seems less likely to be caused by selective cation exchange but may instead reflect higher amounts of electrostatically-bound Y relative to Ho.

Table 2
Summary of mainly extracted phases during sequential leaching.

	Reference materials	Taishir samples	GYZ samples
Fraction 1	Exchangeable and carbonate	Exchangeable and carbonate	Exchangeable and carbonate
Fraction 2	Carbonate	Carbonate	Carbonate
Fraction 3	Carbonate	Carbonate	Carbonate
Fraction 4	Fe–Mn oxide	Fe–Mn oxide	Carbonate, Fe–Mn oxide, phosphate
Fraction 5	Fe–Mn oxide	Fe–Mn oxide	Fe–Mn oxide, phosphate
Fraction 6	Silicate	–	Organic matter and silicate

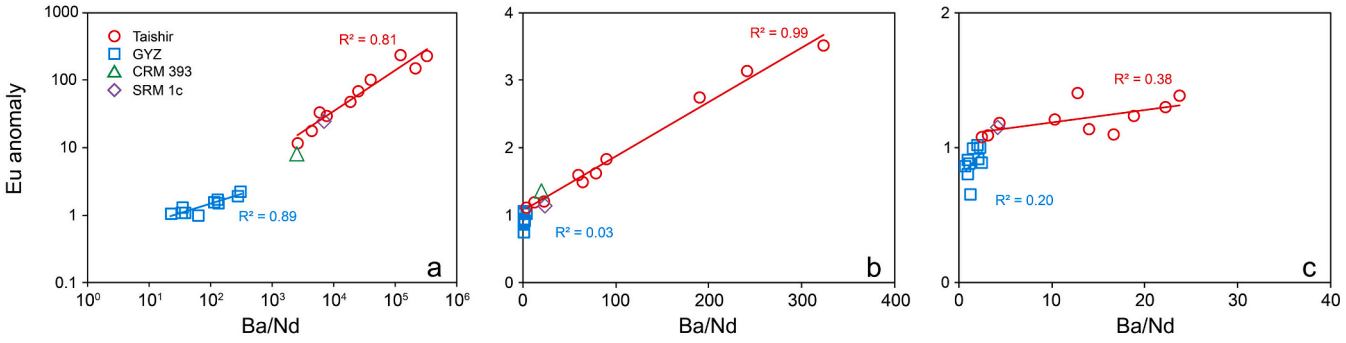

Fig. 9. Cross plots of Eu anomaly against Ba/Nd ratio in all samples and reference materials for (a) fraction 1, (b) fraction 2 and (c) fraction 4. Fractions 1, 2 and 4 are operationally defined as the exchangeable phase, carbonate and Fe–Mn oxide phase, respectively. The Ba/Nd of CRM 393 in fraction 4 is beyond the x-axis range and not shown.

4.1.2. Carbonate phase

It has been demonstrated that partial leaching with 0.3 M acetic acid bears a lower risk of attacking non-carbonate phases (Cao et al., 2020). One might expect that fraction 3 would more likely become contaminated by non-carbonate phases because of the experimental design of excess acid volume and longer leaching time. Intriguingly, for the relatively pure limestones, REE parameters (e.g. Pr_N/Yb_N, Dy_N/Sm_N and Sm_N/Yb_N) show insignificant variability between fractions 2 and 3 even in the case of nearly complete dissolution (Fig. 7). Furthermore, no significant differences in Ce anomaly were observed (Fig. 7). This suggests either that the 0.3 M acetic acid leach used here, following a pre-leach, can mitigate the influence of non-carbonate phases in relatively pure carbonate rocks, or that reliable carbonate-bound REE patterns can be obtained without sequential leaching for pure carbonate rocks (e.g. Shields and Stille, 1998). In this regard, smooth REE patterns exhibiting all the characteristics of modern seawater have been obtained by dissolving detritus-free Holocene microbialites even in 15 N nitric acid (Webb and Kamber, 2000). Nevertheless, considering the slightly elevated REE concentrations and noticeably lower Y/Ho ratio in fraction 3 (Fig. 7), we suggest that the carbonate phase is best represented by fraction 2.

It is observed that the amount of carbonate still remaining after leaching step 3 increases from 0.04% to 32.5% with increasing carbonate rock impurity (Fig. 1). This is due in part to shielding by non-carbonate phases that reduce the active surface area, inhibiting the complete dissolution of carbonate. The larger proportion of undissolved carbonate in GYZ dolostones is also related to the slower reaction kinetics of dolomite relative to calcite (Chou et al., 1989). The mean Mg/Ca ratios gradually increase from 0.17 to 0.45 in GYZ dolostones across the first four fractions (Fig. 10), indicating that calcite is preferentially dissolved over dolomite. Nevertheless, the REE parameters (e.g. Y/Ho, Pr_N/Yb_N, Dy_N/Sm_N and Sm_N/Yb_N) in GYZ dolostones are statistically indistinguishable between fractions 2 and 3 (*t*-tests, *p* values >0.4), which is consistent with previous findings that calcite and dolomite can share similar REE patterns in a dolostone (Zhang et al., 2015). In contrast, Tostevin et al. (2016a) showed that the first leachates of partially dolomitized samples from Brak, Namibia preserve more seawater-like REE patterns. It is possible that the first leachates of Tostevin et al. (2016a) include the exchangeable phase, which then contributed to low REE concentrations and high Y/Ho ratios (Fig. 7). Regardless, it should be mentioned that the dolostones in our study and Zhang et al. (2015) are impure with high siliciclastic contents. Given that their REE patterns are distinct from modern seawater (Fig. 5 and Fig. 2 in Zhang et al., 2015), it is also possible that the dolostone REE patterns have been altered during diagenesis, thus revealing little difference in calcite and dolomite REE patterns (see discussion in Section 4.2).

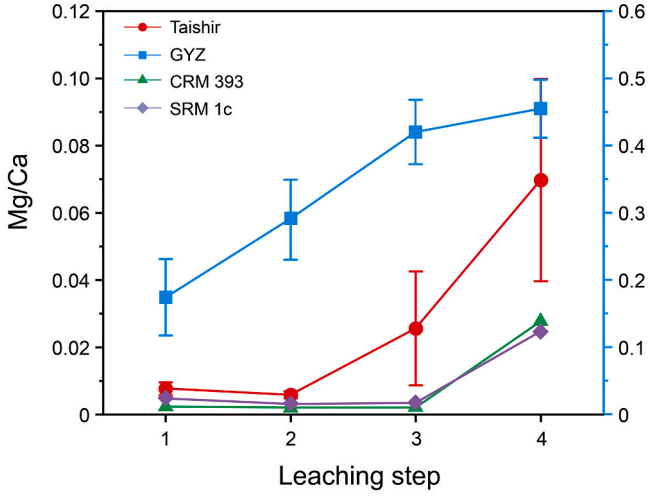

Fig. 10. Variation of Mg/Ca weight ratio in all samples and reference materials across the first four leaching steps. The Taishir and GYZ data are shown as mean values of all samples. Error bars represent ±1 SEM. Note that the y axis scale on the right corresponds to GYZ dolostone data.

It is interesting to note that the major and minor element concentrations (e.g. Fe, Mn, Al, P and K) are consistently higher in impure dolostones than in relatively pure limestones (Fig. 2). The high Fe and Mn concentrations in impure dolostones can be attributed to the dissolution of primary and/or secondary $FeCO_3$ and $MnCO_3$, while the contribution from Fe–Mn oxide dissolution would be limited due to the presence of unreacted carbonates, dilute acetic acid and short reaction time (Poulton and Canfield, 2005). On the other hand, the high concentrations of Al and K likely suggest partial clay leaching. Coincidently, the impure GYZ dolostones exhibit lower Y/Ho ratios and an order of magnitude higher REE concentrations relative to pure carbonate rocks (Fig. 7), which is in line with previous studies suggesting that even dilute acetic acid may attack siliciclastics (e.g. Li et al., 2019). This implies that a weaker acid attack might be needed to extract near primary carbonate-bound REE in impure carbonate rocks, but as discussed above, the high REE concentrations and low Y/Ho ratios are also likely inherited during diagenesis (see discussion in Section 4.2). In addition, there are no significant linear covariations between elements (Al, Fe, Mn and P) and REE patterns in fraction 2, further suggesting that REE patterns are not significantly influenced by dissolution of non-carbonate phases during step 2 (Fig. 11).

4.1.3. Fe–Mn oxide phase

Different sequential extraction schemes have been applied to separate Fe–Mn oxides in soils (Land et al., 1999), modern sediments (Leybourne and Johannesson, 2008), shales (Poulton and Canfield, 2005) and iron formations (Oonk et al., 2018), yet the Fe–Mn oxide phase in ancient carbonate rocks has been surprisingly overlooked so far despite its potential influence on carbonate-bound elements during leaching and/or diagenesis (e.g. Clarkson et al., 2020). Various reductive leaching reagents have been used to extract Fe–Mn oxides (Gutjahr et al., 2007). Following the leaching experiments of Chester and Hughes (1967), the sequential extraction protocol of Tessier et al. (1979) and subsequent method development (e.g. Bayon et al., 2002; Gutjahr et al., 2007), it is now well established that hydroxylamine hydrochloride ($NH_2OH{\cdot}HCl$) in an acid medium can effectively dissolve Fe–Mn oxides. Here, we used 0.1 M $NH_2OH{\cdot}HCl$ in 25% (v/v) acetic acid at room temperature in order not to attack organic matter and siliciclastic phases significantly (Tessier et al., 1979; Filgueiras et al., 2002).

The Fe concentrations increase significantly in the fourth and fifth leaching steps, while the Mn concentrations decrease in the fifth leaching steps for most samples (Fig. 2), suggesting that the more readily reducible Mn oxides were largely removed in fraction 4. The Al concentrations also increase by an order of magnitude, which is attributed to inevitable partial clay leaching due to the presence of a strong acid. Nevertheless, the REE patterns in fractions 4 and 5 are distinct from those in fraction 6, suggesting limited siliciclastic impact. Almost all samples of different purities show characteristic MREE enrichment in the Fe–Mn oxide phase (Fig. 4–6). However, it should be noted that a certain amount of carbonate-bound REE was dissolved in fraction 4 of the GYZ dolostones (Fig. 1). Coincidently, compared with fraction 5, the GYZ dolostones in fraction 4 show relatively less MREE enrichment and lower REE concentrations (Fig. 7) with some revealing similar REE patterns to the carbonate phase (e.g. relatively flat), yet fraction 5 consistently exhibits MREE enrichment and Eu depletion (Fig. 5). Therefore, it can be inferred that carbonate phase dissolution in fraction 4 influences in the REE patterns of GYZ dolostones (see further discussion below).

It is possible that the MREE-enriched patterns of the Fe–Mn oxide phase are induced by artefacts associated with readsorption onto sediment surfaces during sequential leaching. Sholkovitz (1989) showed

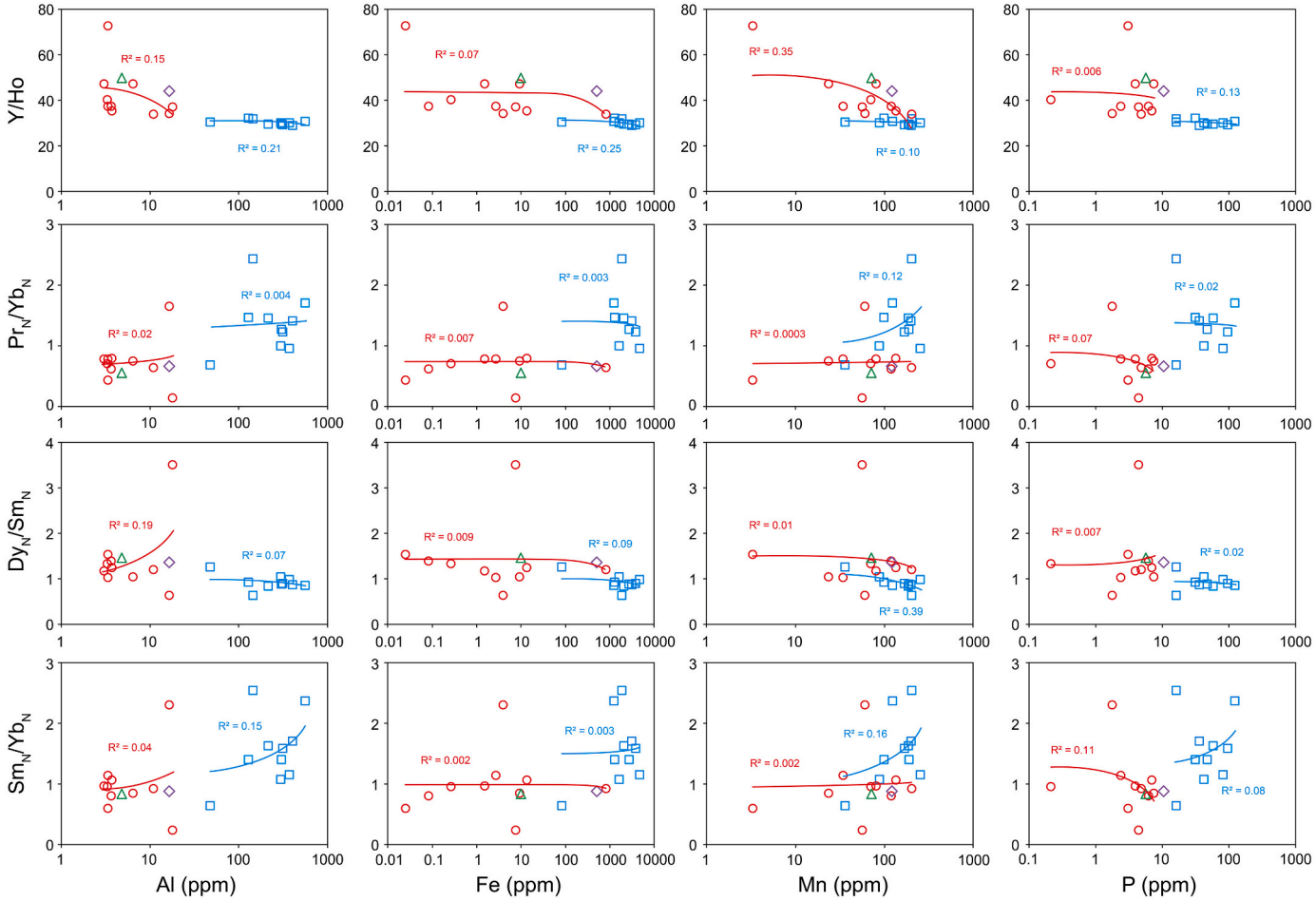

Fig. 11. Cross plots of REE parameters against element concentrations in the carbonate phase (fraction 2) of all samples and reference materials. The red circles, blue squares, green triangle, and purple diamond represent Taishir, GYZ, CRM 393 and SRM 1c, respectively. Note that the x axes are all logarithmically scaled. (For interpretation of the references to colour in this figure legend, the reader is referred to the web version of this article.)

poor recovery (57%) of Eu when leaching 1.0 g of wet muddy sediments (0.5% $CaCO_3$) with 30 ml 0.04 M $NH_2OH{\cdot}HCl$ in 25% (v/v) acetic acid and demonstrated that the readsorption was weakened with decreasing pH and solid/liquid ratio. However, Piper and Wandless (1992) argued against significant readsorption, based on poor REE yields from HCl leaching of pelagic sediments that were pre-treated with 1 M $NH_2OH{\cdot}HCl$ in 25% (v/v) acetic acid. Similarly, Dubinin and Strekopytov (2001) found no evidence for readsorption of REE when dissolving carbonate-lean sediments (<1% $CaCO_3$) in 1 M $NH_2OH{\cdot}HCl$ in 25% (v/v) acetic acid (pH 2) at solid/liquid ratios ranging from 1/800 to 1/67. The readsorption observed in Sholkovitz (1989) has been attributed to the use of muddy sediments possibly rich in organic matter and to the lower molarity of hydroxylamine hydrochloride (Piper and Wandless, 1992). In the case of our study, the lower solution pH (1.6) and low solid/liquid ratio (< 1/100) minimize the likelihood of any readsorption. Furthermore, as readsorption leads to concave-up MREE-depleted and/or LREE-depleted patterns due to preferential adsorption of LREE/MREE by particles and/or organic matter (e.g. Sholkovitz et al., 1994; Pourret et al., 2007), the occurrence of MREE-enriched patterns across all samples (pure, organic-lean, organic-rich) indicates that the MREE-enriched patterns reflect primary signals and not artefacts.

Hannigan and Sholkovitz (2001) have shown that MREE-enriched phosphate minerals can be mobilized under acidic conditions. The acidified hydroxylamine hydrochloride can dissolve phosphorus related to Fe–Mn oxides, but also can release exchangeable P, carbonate-bound P, detrital and/or authigenic P (Poulton and Canfield, 2006). Considering that the exchangeable and carbonate phases have been mostly removed during the first three steps (except for GYZ dolostones), it is conceivable that the reagent may release REE from detrital and/or authigenic apatite, e.g. as francolite nanoparticles (e.g. Shang et al., 2019). The phosphorus concentrations are more than an order of magnitude higher in fractions 4 and 5 than in fractions 2 and 3 (Fig. 2), which is consistent with the dissolution of phosphate minerals. Indeed, the P/(Fe + Mn) ratios exhibit significant positive covariation with REE concentrations of impure GYZ dolostones in fractions 4 and 5, indicating that the leached REE are mainly associated with a dissolved phosphate phase (Fig. 12a). Combined with the discussion above, we therefore suggest that the REE patterns of GYZ dolostones in fraction 4 reflect the joint dissolution effects of carbonates, Fe–Mn oxides and phosphate minerals, while the REE patterns are associated with Fe–Mn oxides and phosphate minerals in fraction 5 (Table 2). The relatively low uranium concentration in fraction 4 (average 1.8 ppm) is attributed to a dilution effect caused by relatively uranium-depleted carbonates and oxide phases. In contrast, for the relatively pure limestones (i.e. Taishir limestones and reference materials), the P/(Fe + Mn) ratios show no covariation with REE concentrations in fraction 4 (Fig. 12b). Although there seems to be a positive covariation between the two parameters in fraction 5 (Fig. 12b), the relationship is significantly controlled by sample T26 with relatively high TOC (0.54%), without which there would be no obvious covariation ($R^2 = 0.0491$). We infer that MREE-enriched patterns in relatively pure limestones are likely related to Fe–Mn oxide dissolution (Table 2).

The characteristic MREE enrichment in the Fe–Mn oxide phase differs from the classic REE patterns of hydrogenetic and diagenetic Fe–Mn

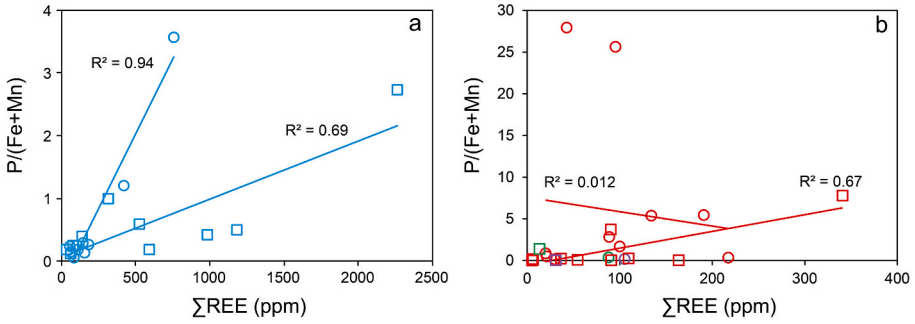

Fig. 12. Cross plots of P/(Fe + Mn) ratio against REE concentration in (a) GYZ dolostones and (b) relatively pure limestones from fraction 4 (circles) and fraction 5 (squares). In panel (b), red, green and purple colours represent Taishir, CRM 393 and SRM 1c, respectively. (For interpretation of the references to colour in this figure legend, the reader is referred to the web version of this article.)

oxides (Bau et al., 2014). Nonetheless, similarly smooth MREE-enriched patterns have been observed in Fe–Mn oxides of ancient carbonates (O'Connell et al., 2020), foraminiferal Fe–Mn coatings (Palmer, 1985) and the Fe–Mn oxide fraction of clastic sedimentary rocks (Johannesson and Zhou, 1999) and modern deep marine sediments (Bayon et al., 2002; Gutjahr et al., 2007), which have been interpreted to be derived from REE exchange with porewater and/or bottom water. However, it should be noted that recent studies also suggest that REE contents of pelagic sediments are mainly hosted in phosphate minerals (bioapatite and carbonate fluorapatite; e.g. Paul et al., 2019; Liao et al., 2022; Deng et al., 2022). Considering the high phosphorus concentrations in the operationally defined oxide fraction of pelagic sediments, it cannot be completely ruled out that the MREE enrichment in some previously investigated pelagic sediments may result from leaching of phosphate minerals instead of Fe–Mn oxides (e.g. Bayon et al., 2002).

Hydrogenetic and diagenetic Fe–Mn oxides are generally characterized by negligible or negative Y anomalies (i.e. Y/Ho < 27) due to the lower stabilities of Y surface complexes (Bau, 1999; Bau et al., 2014). Hydrogenetic Fe–Mn oxides are also often characterized by positive Ce anomalies as a consequence of oxidation of Ce(III) to relatively insoluble Ce(IV) on the oxide surface, the extent of which depends on the growth rate of oxides. In this regard, the negligible to negative Ce anomalies and positive Y anomalies in the Fe–Mn oxide phase of Taishir limestones would then refute the hydrogenetic and diagenetic origins of Fe–Mn oxides (Fig. 7). On the other hand, nearly all modern hydrothermal Fe–Mn precipitates acquire seawater-like REE patterns with positive Eu anomalies due to the initial rapid scavenging of particles during the mixing of seawater and hydrothermal fluid (Bau et al., 2014). The Fe–Mn oxides in Taishir limestones show positive Eu anomalies (average 1.2) that do not covary with Ba/Nd (Fig. 9c), indicating the influence of hydrothermal fluid during their precipitation. However, the Fe–Mn oxide phase is also characterized by MREE enrichment to varying extents (Fig. 4), which seems to conflict with a solely hydrothermal origin. Hydrothermal Fe–Mn oxides, if exposed to seawater after initial precipitation, would tend to evolve toward hydrogenetic-like patterns (i.e. Ce enrichment and reduced Y/Ho ratios) because of continuous scavenging from ambient seawater (Bau et al., 2014). Given that the Fe–Mn oxides from the upper strata of Taishir limestones still bear some resemblances with the modern seawater pattern (Fig. 4), we infer that the Fe–Mn oxide REE patterns may reflect further exchange, surface and solution complexation with marine-derived fluids after initial precipitation. The negative covariation ($R^2 = 0.58$; not shown) between Ce anomalies and Y/Ho ratios in fraction 4 provides further support for the inference. Consequently, the slight LREE/MREE enrichment can be attributed to less HREE adsorption during continuous scavenging, which is also consistent with the REE partition coefficients between Fe–Mn oxides and seawater (Koeppenkastrop and De Carlo, 1992; Ohta and Kawabe, 2001; Quinn et al., 2006; Schijf and Marshall, 2011). Taken together, we suggest that the Fe–Mn oxides in Taishir limestones are of hydrothermal origin yet experienced prolonged exchange with seawater.

It is interesting to note that the seawater-like REE pattern reappears in fraction 5 of CRM 393. The leachate was shown to exhibit the same pattern twice in different batches, ruling out the possibility of an analytical artefact. The acidified hydroxylamine hydrochloride is effective in dissolving Mn oxides and easily reducible amorphous Fe oxides but less so for crystalline Fe oxides (e.g., goethite, hematite, and magnetite) (Kheboian and Bauer, 1987; Kim and Fergusson, 1991; Chassé et al., 2019). It has been demonstrated that a 48-h extraction using 1 M $NH_2OH{\cdot}HCl$ in 25% (v/v) acetic acid removes <1% of goethite and magnetite (Poulton and Canfield, 2005). It is therefore possible that poorly reducible Fe oxides, if they exist, were extracted in fraction 5 after most of the easily reducible Mn and Fe oxides were released in fraction 4, which is also consistent with decreased Mn concentrations in most samples in fraction 5. As shown in Fig. 1, the decreased Mn and P concentrations and very low U concentration in fraction 5 of CRM 393 suggest limited influence of Mn oxides and phosphate. Consequently, the seawater-like REE pattern possibly derives from crystalline Fe–-oxides and likely indicates that the oxides precipitated under oxic conditions and had limited exchange with ambient fluids once formed (Slack et al., 2007; Bau et al., 2014). If correct, our results would suggest that similar to the carbonate phase, distinct Fe oxide phases also occur in carbonate rocks.

4.1.4. *Organic matter/silicate phase*

The important role of organic matter in REE cycling in Earth's surface environment has long been recognized (e.g. Elderfield et al., 1990; Sholkovitz et al., 1994; Freslon et al., 2014), yet organic matter REE patterns remain poorly explored, due in part to the complex origins and composition of organic matter (Zhang and Shields, 2022). The stability constants of REE upon complexation with organic ligands vary with functional groups of organic ligands (e.g. Byrne and Li, 1995), and are also influenced by fluid pH and ionic strength (e.g. Zoll and Schijf, 2012; Schijf and Byrne, 2021). The active uptake of LREE by organisms (e.g. aerobic methanotrophs) due to their presence in the active site of methanol dehydrogenase (Picone and Op den Camp, 2019; Meyer et al., 2021) further complicates the interpretation of organic matter REE patterns, but also opens the door for the use of REE in identifying microbial activities in modern environments and/or geological past (e.g. Bayon et al., 2020a). On the other hand, since the commonly used reagents to oxidize organic matter can attack other phases as well (Filgueiras et al., 2002), the resultant 'organic matter' REE patterns may reflect a combination of different phases (Table 2). As shown in Fig. 2, the Al (and K) concentrations increase by an order of magnitude from fractions 5 to 6 in GYZ dolostones and reference materials, suggesting partial leaching of silicate minerals due to the presence of 10% HNO_3. Therefore, the LREE enrichment in the CRM 393 and SRM 1c that are devoid of organic matter reflect the characteristics of the more labile

silicate fraction (Table 2). Assuming that the dissolved silicates in the GYZ dolostones also exhibit LREE enrichment, the organic matter in the GYZ may be characterized by HREE enrichment given the reverse variations of Dy_N/Sm_N, Pr_N/Yb_N and Sm_N/Yb_N ratios between reference materials and GYZ dolostones in fraction 6 (Fig. 7). However, the REE patterns of dissolved silicates depend on the mineral assemblages in the residual fraction, which is ultimately controlled by local geology, e.g. HREE enrichment in the insoluble fraction of the lower Cambrian carbonate rocks in South China (Gong et al., 2021). Therefore, the organic matter REE patterns in the GYZ dolostones remain inconclusive. Future studies aided by well-developed methods to separate organic matter from other phases would be needed to better understand organic matter REE patterns.

4.2. Origin of carbonate REE patterns

The carbonate phase REE patterns in Taishir limestones reveal a stratigraphic trend whereby lower strata are mostly characterized by LREE/MREE enrichment and upper strata show seawater-like patterns (Shields et al., 1997; Shields et al., 2002). As discussed above (Section 4.1.2), these non-seawater-like REE patterns are not derived from leaching of non-carbonate phases, but may reflect syn- and/or post-depositional mixing of different fluids. It has been proposed that the relatively flat REE patterns in some Neoproterozoic carbonate rocks reflect freshwater input during deposition (e.g. Frimmel, 2009; Zhao et al., 2009). Although freshwater has relatively higher REE concentrations with respect to seawater, a large proportion of freshwater REE will be sequestered into sediments during estuarine mixing due to salt-induced colloidal flocculation (Sholkovitz, 1993). Nevertheless, complexation with carbonate ions in alkaline rivers and with dissolved organic matter can lead to diminished REE removal (Merschel et al., 2017; Adebayo et al., 2018; Bayon et al., 2020b). Snow meltwater and coastal seawater characterized by MREE enrichment have also been reported from Marian Cove in the Antarctic (Kim et al., 2015). Considering that the lower part of the section was deposited in the aftermath of Sturtian glaciation, it needs to be considered whether these rocks were influenced by glacial meltwater during deposition. The Taishir limestones are interpreted to have been deposited in a distal marine environment and retain the Sr isotope composition of contemporaneous seawater (Shields et al., 2002; Bold et al., 2016). We therefore argue that any significant impact from freshwater on the Taishir limestones is unlikely. Furthermore, petrographic observations suggest that the carbonate rocks are dominated by microspar without significant late diagenetic recrystallization.

MREE- and LREE-enriched patterns have been interpreted to reflect primary seawater chemistry (e.g. Lécuyer et al., 2004; Emsbo et al., 2015; Hood and Wallace, 2015). Based on detailed petrographic studies, Hood and Wallace (2012) suggested that dolomitic cements in the Cryogenian Balcanoona Formation precipitated during early marine diagenesis, perhaps within one meter below the sediment-water interface. They proposed that coupled with less scavenging of hydrothermally derived REE, Fe–Mn oxide reduction below the redox chemocline in the water column led to MREE enrichment in both seawater and diagenetic cements. However, no such pattern has been observed in modern anoxic basins, while conversely the positive Ce anomalies that are generally observed in anoxic seawater of modern redox-stratified basins (e.g. Schijf et al., 1995; De Baar et al., 1988) and/or oxic waters of extreme alkalinity (e.g. lake waters; Möller and Bau, 1993; Johannesson et al., 1994) have seldom been found in those carbonate rocks, with one Cryogenian exception being the Ringwood Member of the Aralka Formation, which exhibits LREE depletion (Verdel et al., 2018). Marine cements from the laterally equivalent Angepena Formation in the Adelaide Fold Belt also exhibit characteristic MREE enrichment (O'Connell et al., 2020), but were deposited in a relatively oxidizing peritidal environment, suggesting that MREE-arching patterns develop irrespective of sedimentary facies. Therefore, further arguments are needed to infer a primary seawater origin for MREE-arching patterns.

Excluding a fluid mixing, late diagenetic or primary seawater origin leads us to suggest that LREE- and MREE-enriched patterns reflect the influence of early diagenetic remobilization. Numerous studies have demonstrated REE mobility in marine porewaters during early diagenesis, leading to several orders of magnitude higher REE concentrations below the sediment-water interface (from several centimetres to metres) than in the overlying seawater (e.g. Elderfield and Sholkovitz, 1987; Haley et al., 2004; Kim et al., 2012; Abbott et al., 2015; Deng et al., 2017). This is mainly attributed to the decomposition of organic matter and dissolution of Fe–Mn oxides (and/or detritus) during early diagenesis, releasing REE back into porewaters. (e.g. Haley et al., 2004; Abbott et al., 2019). Porewater REE patterns are ultimately controlled by diverse sources, sinks and accompanying fractionation processes, and so it may not be surprising that a range of REE patterns, e.g. flat, LREE enrichment, MREE enrichment and HREE enrichment, have all been reported from marine porewaters at different depths in different depositional settings (Haley et al., 2004; Kim et al., 2012; Himmler et al., 2013; Abbott et al., 2015; Deng et al., 2022). The mobility of REE during early diagenesis is also evidenced by extensive authigenic carbonate precipitation at cold seeps and early diagenetic foraminiferal coatings, the REE patterns of which resemble their ambient porewaters (Rongemaille et al., 2011; Bayon et al., 2011; Skinner et al., 2019; Bayon et al., 2020a). Given the similar REE patterns of some carbonate and Fe–Mn oxide phases (Figs. 4, 5), we consider that these non-seawater-like REE patterns may also have formed during early diagenesis (Fig. 13). Fe–Mn oxide (and/or organic matter) particle fluxes to the seafloor can vary considerably, and potentially dominate REE concentrations in shallow porewaters (perhaps a few to tens of centimetres below the sediment-water interface). Under fluid-buffered conditions, the REE patterns of the carbonate phase may be strongly affected by REE-enriched porewaters.

To test the hypothesis, we conducted a simple open system fluid-rock interaction modelling (after Banner and Hanson, 1990) tracing the evolution of carbonate REE patterns during early diagenesis. The modelling parameters and assumptions can be found in the Supplementary Material. We first simulated how modern seawater and porewater would modify REE patterns of carbonate sediments primarily deposited under oxic conditions (represented by CRM 393 from this study) and suboxic-anoxic conditions (represented by GRE1/48 from Tostevin et al., 2016b). As shown in Fig. 14, the modelling suggests that interaction with modern oxidizing seawater will not significantly modify the REE signatures even at a fluid/rock ratio of 10^4, which is consistent with the result of Banner et al. (1988). The very low fluid REE/Ca ratios can account for the resistance of carbonate sediments to seawater alteration. This may also explain the preservation of seawater-like REE patterns in diagenetic carbonates that interacted with a seawater-like fluid (e.g. Liu et al., 2019). In contrast, the REE signatures are mobilized at relatively low fluid/rock ratios (10^2–10^3) when interacting with reducing porewaters and become progressively enriched in LREE/MREE with increasing fluid/rock ratios, as evidenced by the evolutionary trajectories of Pr_N/Yb_N and Dy_N/Sm_N ratios (Fig. 14e, f). The resultant REE patterns are similar to those reported by Hood and Wallace (2015) and O'Connell et al. (2020), suggesting that early diagenesis can also induce LREE- and MREE-enriched patterns. Importantly, the Ce anomalies of both rocks also appear to be affected by the diagenetic fluid (close to unity in this case; Fig. 14d), which could potentially explain the absence of pronounced positive Ce anomalies in many LREE/MREE enriched carbonates (and phosphorites).

We further simulated the influence of early diagenesis on the REE patterns of the lower Taishir limestones (Fig. 14b, c), by assuming that the adjacent sample (T8), characterized by a seawater-like REE pattern, represents a primary marine signature. The dissolution of Fe–Mn oxides is assumed to have dominated the porewater REE, and therefore the REE patterns of the Fe–Mn oxide phase (fraction 4) in corresponding samples

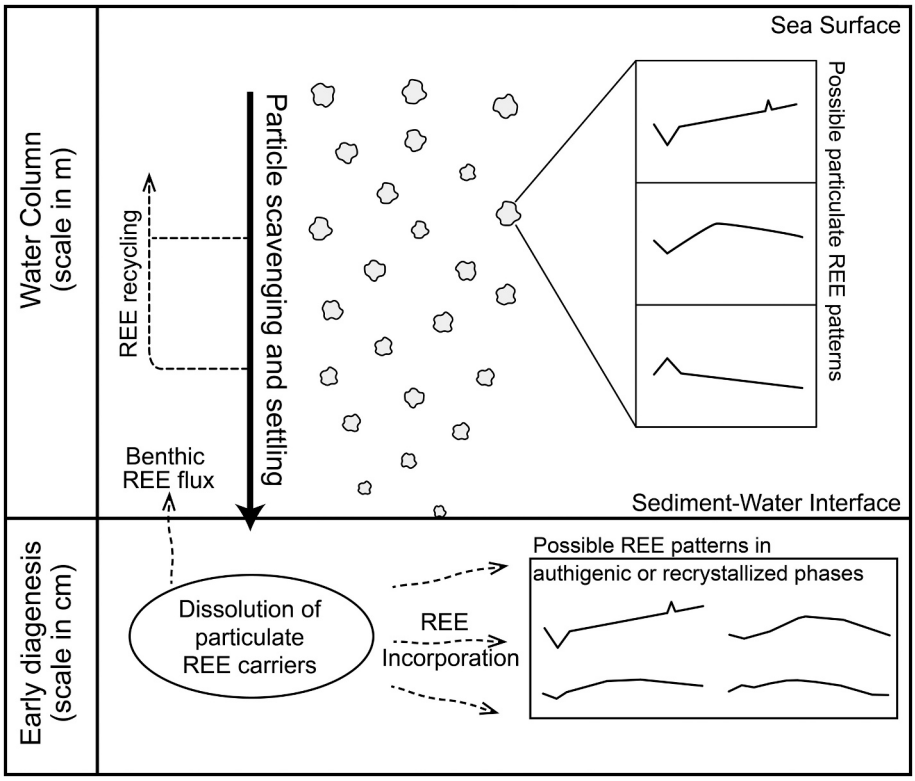

Fig. 13. A conceptual diagram illustrating the REE particulate flux to the seafloor and subsequent dissolution during early diagenesis. The REE patterns in the diagram are illustrative only. The REE carrier phases comprise detrital minerals, organic matter and biominerals and marine precipitates such as oxides and silica. Partial decomposition and/or dissolution during downward settling results in REE recycling in the water column. Once the particles reach the seafloor, they will undergo either oxic degradation or anoxic remineralization and/or dissolution, elevating shallow porewater REE concentrations, modifying porewater REE patterns, and overprinting REE patterns of authigenic or recrystallized phases upon incorporation.

represent porewater REE patterns. The porewater REE concentrations are further assumed to be 10^{-4} times lower than that of the Fe–Mn oxide phase to reach a comparable level to modern porewaters. As shown in Fig. 14b and c, the key features of carbonate REE patterns, e.g. MREE bulge and LREE enrichment, are well reproduced by diagenetic modelling at a fluid/rock ratio of 3000, reinforcing the possibility that carbonate REE patterns deviate from seawater and/or their original patterns during early diagenesis. Nevertheless, we note that there are certain discrepancies between simulated REE patterns and measured carbonate patterns, e.g. less LREE enrichment, which we attribute to using the same porewater REE patterns as the Fe–Mn oxide phase. Indeed, decomposition of organic matter during early diagenesis is also an important REE source in shallow porewaters (Freslon et al., 2014), which presumably would first release LREE scavenged in the water column (Haley et al., 2004). This additional source of LREE may explain the discrepancy between our modelled and measured carbonate phase REE patterns. Different partitioning behaviours of REE between solution and calcite under different aquatic chemistry might also contribute to LREE enrichment but this remains highly unconstrained (e.g. Zhong and Mucci, 1995; Toyama and Terakado, 2014; Voigt et al., 2017). In addition, compared with the simulated REE patterns, sample T11 has much lower REE concentrations, which can be reconciled by early cementation of authigenic carbonate. While the diagenetic model adopted here (Banner and Hanson, 1990) assumes no net volume change of carbonates (i.e. complete dissolution and reprecipitation at each iteration step), authigenic carbonate precipitation during early diagenesis due to increased alkalinity by anaerobic oxidation of organic matter/methane would occupy the pore space gradually. Authigenic carbonates are generally depleted in REE (Himmler et al., 2010; Rongemaille et al., 2011) and so a mixture of authigenic carbonates and recrystallized carbonates may account for the relatively low measured REE concentrations.

Our results seem to contradict those of Liu et al. (2019) who demonstrated that early marine diagenesis would not significantly alter the primary REE patterns of carbonate rocks. However, as mentioned above, this is mainly because the diagenetic fluids for Bahamian carbonates are chemically similar to seawater with respect to their REE signatures (Liu et al., 2019). On the other hand, early diagenetic alteration of REE patterns might not always be evident (Skinner et al., 2019), but could depend on sedimentation rates that influence the residence time of porous carbonate sediments in the early diagenetic zone, on bottom water oxygen penetration depth, and on the flux of organic matter or other REE carrier phases to the seafloor. The discrepancy may also be related to the mineralogy, styles and loci of carbonate precipitation, which have changed markedly throughout Earth's history. The primary polymorphs of marine carbonate have oscillated between aragonite and calcite through the Proterozoic to the Phanerozoic due to seawater chemistry variation (e.g. Sandberg, 1983; Hardie, 2003). Aragonite is metastable and tends to transform into more stable low-Mg calcite (neomorphism) under most surface conditions, during which the primary geochemical signal can be modified (e.g. Brand and Veizer, 1980; Morse et al., 2007). Webb et al. (2009) demonstrated that REE were mobilized during meteoric neomorphism, although the REE patterns remained unaltered due to the low REE concentration of the ambient fluid. On the other hand, carbonate precipitation was triggered by abiotic and microbial processes before the appearance of biomineralization (Grotzinger and James, 2000). Diverse carbonate textures (e.g. crystal fans, molar tooth calcite, intraclasts and giant ooids) have been observed to dominate carbonate sediments in different parts of the Precambrian (see Cantine et al. (2020) for a review). Although the causes of the secular trend of carbonate precipitation remain ambiguous (e.g. Shields, 2002; Higgins et al., 2009), it implies that many carbonate sediments formed at or below the sediment-water interface in the Precambrian (Cantine et al., 2020), and likely underwent chemical exchange with porewaters or directly inherited porewater chemistry during early diagenetic recrystallization or cementation. In contrast, the Bahamian carbonates in the Clino and Unda cores are dominated by reefal and skeletal deposits (Eberli et al., 1997; Liu et al., 2019). Although the utility of REE chemistry in skeletal carbonates is still contentious (Tostevin et al., 2016a; Li et al., 2019), it is generally

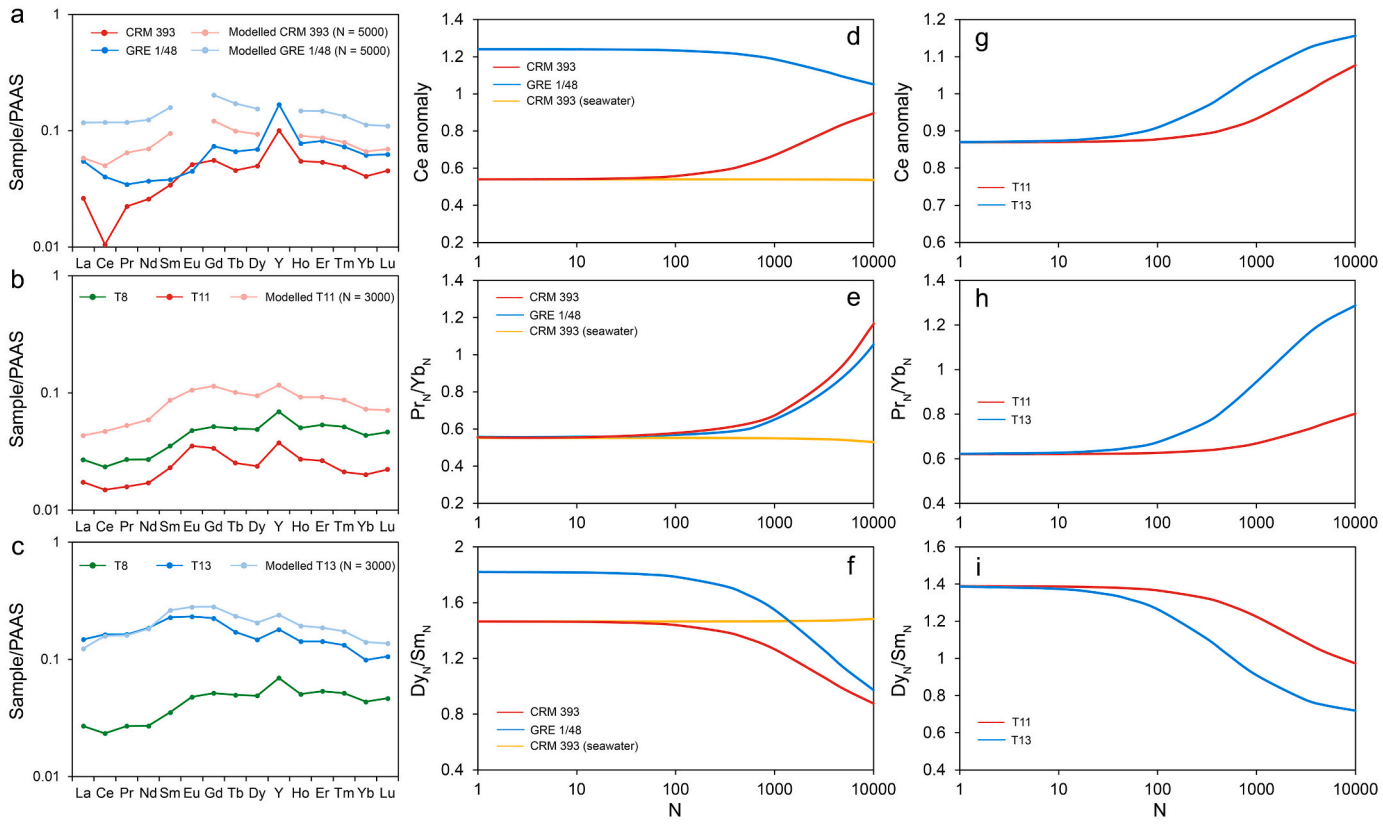

Fig. 14. Open-system fluid-rock interaction model for REE in carbonate rocks. N is the cumulative fluid to rock ratio. (a-c) Comparison of measured REE patterns and modelled REE patterns. While panel (a) shows the alteration of REE patterns in carbonate rocks interacting with the modern porewater (data from Abbott et al., 2015), panels (b) and (c) show the results of the interaction of primary carbonate rock with assumed porewaters, the REE patterns of which are the same as the corresponding Fe–Mn oxide phase. T8 represents the assumed primary carbonate REE pattern. (d-f) Evolution of REE parameters in CRM 393 and GRE 1/48 during interaction with modern oxidizing seawater (light brown line) and porewater. (g-i) Evolution of REE parameters in T11 and T13 during interaction with assumed porewaters. (For interpretation of the references to colour in this figure legend, the reader is referred to the web version of this article.)

accepted that they acquire their initial chemical signature directly from a fully oxic water column. Consequently, their residence time in more reducing, early diagenetic porewaters might be relatively short, leading to a greater likelihood of preserving an open seawater signature. Nonetheless, it should be noted that sparse Ce anomaly values greater than 0.8–0.9 in the Bahamian carbonates (Liu et al., 2019) are not representative of modern oxygenated seawater but possibly signal early diagenetic exchange.

German and Elderfield (1990) proposed that seawater REE signatures are more likely preserved in sediments under oxic diagenesis, whereas anoxic early diagenesis tends to alter the REE patterns and Ce anomalies of sediments, highlighting the redox cycling of REE in marine porewaters. Nevertheless, very seawater-like REE patterns have been observed in carbonate rocks and iron formations that were deposited in a fully anoxic ocean (e.g. Kamber and Webb, 2001; Oonk et al., 2018), while conversely, non-seawater-like REE patterns have been observed in Cryogenian iron-oxide-rich carbonate rocks deposited in an oxidized peritidal environment (O'Connell et al., 2020). It thus appears that the preservation of seawater REE signatures in carbonate rocks is controlled less by the redox conditions of the water column and/or porewater, but instead more by the spatiotemporally heterogeneous flux of REE carrier phases to the seafloor and their subsequent dissolution in porewater. In this regard, REE patterns and concentrations can be used to identify overprinting of seawater REE signatures. Taking the Taishir limestones as an example (Fig. 15), the sample with the most seawater-like REE pattern is characterized by low REE content, low Pr_N/Yb_N and Sm_N/Yb_N ratios, high Dy_N/Sm_N and Y/Ho ratios. Accompanied by increasing REE concentrations, the patterns gradually deviate from most seawater-like, with the samples that exhibit non-seawater-like patterns having the highest REE contents (Fig. 15). This is consistent with incorporation of REE during early diagenetic recrystallization (Fig. 14), while the non-seawater-like pattern with low REE content likely reflects authigenic carbonate precipitation in shallow porewaters (Fig. 15). Therefore, covariation diagrams combining REE concentrations and REE pattern parameters (Fig. 15) show great promise for identifying overprinting of seawater REE signatures.

The GYZ dolostones are all characterized by non-seawater-like REE patterns in the carbonate phase. The remarkable similarity of REE patterns between the carbonate phase and other phases (as expressed in fractions 4 to 6) in GYZ dolostones implies an intrinsic relationship (Fig. 5). Indeed, dolomitization of original GYZ carbonate sediments would require open system water-rock interaction with the Mg^{2+} enriched solution during either early or late diagenesis, while dolomitization itself may further increase rock porosity due to reduction of rock volume (e.g. Weyl, 1960). Authigenic apatite crystals identified in Member III of the Gaoyuzhuang Formation (Shang et al., 2019) further suggest that there could have been intense organic matter remineralisation during their deposition. It therefore can be inferred that their REE patterns may also have been altered during early diagenesis, although we cannot fully exclude the influence of late diagenesis. Interestingly, the REE patterns of different host phases in the Gaoyuzhuang Formation are all characterized by prevalent Eu depletion (Fig. 5), which is not commonly observed in carbonate rocks, and this is further discussed in the following section.

4.3. Negative Eu anomalies

Due to the extremely low redox threshold for reducing Eu^{3+} to Eu^{2+},

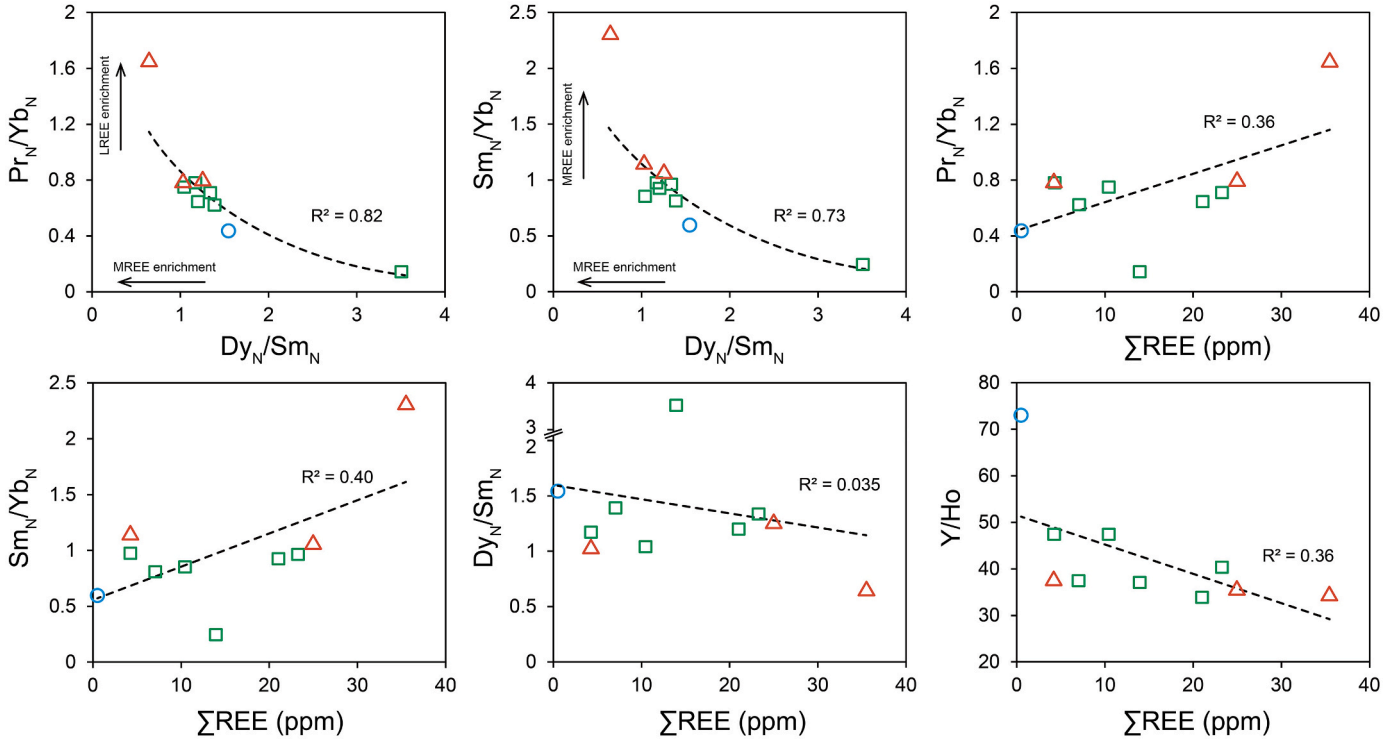

Fig. 15. Covariation diagrams of REE parameters (fraction 2) in Taishir limestones. Blue circle indicates a very seawater-like REE pattern, while red triangles indicate non-seawater-like REE patterns. Green squares represent samples that retain modern seawater REE characteristics to some extent. (For interpretation of the references to colour in this figure legend, the reader is referred to the web version of this article.)

it would be difficult to reduce trivalent Eu in normal surface environments, but higher temperatures favour reduction, thus leading to fractionation of Eu with respect to the other REE, as seen in modern high-temperature hydrothermal fluids (Michard and Albarède, 1986; Elderfield, 1988; Bau, 1991). Therefore, positive Eu anomalies in ancient banded iron formations and carbonate rocks are commonly attributed to hydrothermal influence (e.g. Kamber and Webb, 2001). Theoretical considerations suggest that Eu^{3+} reduction might occur at lower temperatures in extremely reducing, highly alkaline environments, in which sulfate reduction had nearly reached completion (Sverjensky, 1984). It has therefore been proposed that Eu can be mobilized in porewaters of anoxic marine sediments (MacRae et al., 1992). However, the absence of Eu anomalies in the methanogenic zone of pore fluids would appear to refute early diagenetic remobilization of Eu (Kim et al., 2012).

By contrast, negative Eu anomalies are most commonly found in intermediate and felsic volcanic rocks due to preferential incorporation of Eu^{2+} into feldspar (Weill and Drake, 1973; Hanson, 1980). Interestingly, the negative Eu anomalies are not only found in GYZ carbonate rocks at Gan'gou section (this study) but also at Jixian section (Zhang et al., 2018), implying a regionally significant process. It has been proposed that hydrothermal alteration can lead to the preferential removal of Eu and leave behind a negative Eu anomaly in host rocks (Sverjensky, 1984; Bau and Möller, 1992). Although a slightly negative Eu anomaly has been found in burial-dolomite samples (Hood et al., 2018), we consider it less likely for GYZ carbonate rocks owing to the lack of evidence for significant recrystallization (Zhang et al., 2018; Shang et al., 2019). Although Eu depletion could reflect the dissolution of specific phases into porewaters, given the regional nature of these anomalies and their persistence through Fe–Mn oxide, phosphate and organic matter/silicate phases (Fig. 5), it seems more likely that it was a general feature of local seawater. In this regard, Kamber et al. (2004) has noted the disappearance of negative Eu anomalies in stromatolites when normalised to local tonalite. Considering that widespread anorogenic magmatism during ~1.76–1.65 Ga produced considerable amounts of extrusive felsic volcanic rocks in North China (Zhai et al., 2015), the negative Eu anomalies could reflect the weathering of intermediate-felsic rocks, something which could be tested for by future studies on shales from the same stratigraphic successions. Overall, negative Eu anomalies are uncommon in carbonate rocks and could signal either strong local effects in restricted seaways or diagenetic exchange with siliciclastic material. Consequently, significant negative Eu anomalies in carbonate rocks should be interpreted with caution.

4.4. *The conundrum of $\delta^{13}C$ excursions with non-seawater-like REE patterns*

The Neoproterozoic Era is characterized by sustained high $\delta^{13}C$ values punctuated by extraordinary negative $\delta^{13}C$ excursions, and yet the mechanisms to explain both high background values and negative anomalies remain controversial. The negative excursions have been proposed to be a primary feature of seawater, related possibly to the oxidation of a ^{13}C-depleted carbon reservoir (e.g. dissolved organic carbon or methane: Rothman et al., 2003; Bjerrum and Canfield, 2011; Shields et al., 2019), or early and/or late diagenesis (e.g. Derry, 2010; Schrag et al., 2013; Cui et al., 2017). The long-lived high mean $\delta^{13}C$ values have been traditionally interpreted to reflect high fractional organic carbon burial (Knoll et al., 1986; Canfield et al., 2020), which could relate to low rates of physical erosion (Shields and Mills, 2017), but might also reflect elevated rates of authigenic carbonate formation (Schrag et al., 2013). Interpreting the carbonate $\delta^{13}C$ record is beyond the scope of this study, but there is an apparently unresolved conundrum that the negative $\delta^{13}C$ excursions preserved in Neoproterozoic carbonate rocks are generally associated with non-seawater-like REE patterns. For example, the Tonian Bitter Springs Formation in the Amadeus Basin of Central Australia is characterized by an interval of negative $\delta^{13}C$ values (Bitter Springs anomaly: Hill and Walter, 2000; Halverson et al., 2020), whilst the corresponding stromatolites exhibit LREE-enriched patterns with positive La anomalies (Corkeron et al., 2012). The Cryogenian

Trezona Formation in the Flinders Ranges of South Australia contains a negative carbon isotope excursion with $\delta^{13}C_{carb}$ values approaching −10‰ (Trezona anomaly: Rose et al., 2012), whereas the REE patterns show characteristic MREE enrichment (Ward et al., 2019). The REE patterns of the Ediacaran Wonoka Formation in the Adelaide Rift Complex of South Australia that preserves the Wonoka/Shuram anomaly are mostly characterized by MREE enrichment (Ward et al., 2019). Similarly, Member III of the Doushantuo Formation in the Yangtze Gorges area of South China that records the Shuram anomaly exhibits relatively flat REE patterns with positive La anomalies (Ling et al., 2013; Zhao et al., 2021).

If the carbonate $\delta^{13}C$ record represents primary seawater chemistry, one would predict that the carbonate rocks should also preserve seawater-like REE patterns (except for Ce, which is redox controlled) based on the long-standing viewpoint that REE patterns in carbonate rocks are resistant to diagenetic alteration. Indeed, a diagenetic origin for the negative carbon isotope anomalies is perhaps less likely in light of the globally correlative nature of negative $\delta^{13}C$ excursions and petrographic evidence (Canfield et al., 2020; Yang et al., 2021; Cui et al., 2021). One possible explanation for this apparent contradiction is that the non-seawater-like REE patterns were produced during sample digestion due to the dissolution of non-carbonate phases by strong acid leaching (e.g. Frimmel, 2009, 2010). However, several studies based on more gentle leaching methods (e.g. acetic acid digestion) failed to produce seawater-like REE patterns (Ling et al., 2013; Ward et al., 2019; Zhao et al., 2021). Alternatively, although the carbonate $\delta^{13}C$ record is also influenced by local environments, the shorter residence time of REE in the ocean (10^2–10^3 vs. 10^5 yrs. of carbon) makes them more susceptible to local processes. Therefore, it has been proposed that the non-seawater-like REE patterns could reflect either freshwater input or locally restricted environments (Kamber and Webb, 2001; Frimmel, 2010; Bolhar et al., 2015; Zhao et al., 2021). However, freshwater REE are largely removed (60–80% removal) along with the development of typical open marine REE patterns during estuarine mixing (e.g. Lawrence and Kamber, 2006). Furthermore, the Wonoka, Doushantuo and Trezona formations are all interpreted to represent open marine deposition (Haines, 1988; Jiang et al., 2011; Rose et al., 2012), rendering less likely any potential influence from freshwater. The late diagenetic origin of non-seawater-like REE patterns is perhaps the least likely alternative because it would easily be discernible from petrographic observation (Cui et al., 2021). By excluding the other alternatives and given the modelling evidence that REE are particularly susceptible to exchange with shallow porewaters, we suggest that these non-seawater-like REE patterns associated with primary negative $\delta^{13}C$ excursions are most parsimoniously explained by early diagenetic exchange. As discussed above, the REE patterns of carbonate sediments are commonly governed by exchange with shallow REE-enriched porewaters, which are in turn controlled by the flux of REE carrier phases to the seafloor (Fig. 13). During the critical intervals, the local shallow porewater REE concentrations could have been high due to a regionally high particle flux, under which conditions the REE features of carbonates, whether directly precipitated or recrystallized during syndepositional processes, would be strongly affected by shallow REE-enriched porewaters. Conversely, shallow porewaters may be buffered by a large marine dissolved inorganic carbon (DIC) pool, thus preserving near-primary carbon isotope records in the same carbonate sediments (see also discussion below).

More recently, Lau and Hardisty (2022) proposed that I/Ca and Ce anomaly represent the most likely and least likely altered redox proxies in carbonate sediments, respectively, implying that high I/Ca values give credence to other proxies, whereas alteration of Ce anomalies would imply alteration of most other proxies. This inference is, to some extent, supported by studies of ancient and modern carbonate sediments. For instance, although characterized by seawater-like REE patterns, the U isotope ratios of Bahamian carbonate sediments have been altered by early diagenesis to heavier values than seawater by +0.27 ± 0.14‰ (Chen et al., 2018; Liu et al., 2019). Similarly, seawater-like REE patterns in the Belcher Group from Canada are associated with anomalous $\delta^{98}Mo$ values lower than the crustal range (Hodgskiss et al., 2021). Hood and Wallace (2012) noted that syndepositional (early marine diagenetic) dolomite cements characterized by MREE enrichment exhibit slightly lower carbon isotope values than primary carbonates (mean difference of 1.6‰). However, the opposite case also exists. Elevated I/(Ca + Mg) values greater than 0.5 μmol/mol have been observed in conjunction with non-seawater-like REE patterns in Mn-rich carbonates of Member II of the Gaoyuzhuang Formation (Fang et al., 2020). This discrepancy may be related to the underestimated role of Fe–Mn oxides in the diagenetic modelling of Lau and Hardisty (2022). Furthermore, the carbonate carbon isotopes of Taishir limestones in Mongolia show scant evidence of significant diagenetic alteration and are reproducible across large areas despite significant facies changes (Shields et al., 2002; Johnston et al., 2012; Bold et al., 2016), although some of their REE patterns clearly deviate from that of modern seawater (Fig. 4). Remarkably, the Taishir limestones also preserve the contemporaneous seawater Sr isotope composition (Shields et al., 2002; Bold et al., 2016), exhibiting comparable values to the Rasthof Formation in Namibia (Yoshioka et al., 2003) and the Twitya Formation in Canada (Rooney et al., 2014). The co-occurrence of non-seawater-like REE patterns and primary carbon and strontium isotope ratios is intriguing because their relative resistance to diagenesis contradicts expectation (e.g. Banner et al., 1988; Lau and Hardisty, 2022). We consider that this is because although carbonate REE patterns are influenced by Fe–Mn oxide dissolution during early diagenetic (syndepositional) processes, the $^{87}Sr/^{86}Sr$ isotope ratios could remain unaltered in the absence of significant detritus dissolution. Likewise, although Fe–Mn oxide dissolution could be accompanied by organic matter decomposition, the pore fluids in the syndepositional environment may be dominated by the large marine DIC pool, and consequently, the carbonate carbon isotopes remain largely intact. This could also potentially explain the non-seawater-like REE patterns in Member III (Shuram anomaly) of the Doushantuo Formation in the Yangtze Gorges area, which preserves primary carbon and strontium isotope ratios (Sawaki et al., 2010; Yang et al., 2021). The globally correlative $\delta^{34}S_{CAS}$ and $\delta^{238}U$ values of Member III (Shuram anomaly) imply that these isotopic systems can also potentially preserve near primary values despite non-seawater-like REE patterns (Cui et al., 2015; Zhang et al., 2019; Shi et al., 2022; Dodd et al., 2023). Taken together, this indicates that the traditionally considered resistant proxy, REE, is indeed sensitive to early diagenetic alteration and that proxies' sensitivities to early diagenetic (or syndepositional) processes are variable for different systems and under different local conditions. Therefore, we suggest that carbonate REE patterns should not be viewed as a general indicator of the preservation of geochemical parameters and that alteration of isotopic systems should be evaluated independently.

4.5. Implications for carbonate-bound REE as a redox proxy

The REE patterns in carbonate rocks are an informative proxy for paleo-seawater chemistry and local-regional redox conditions and have been extensively applied to infer paleoenvironments. The reliable interpretation of carbonate REE patterns firstly builds upon the application of robust leaching methods. Sequential leaching of carbonate fractions suggests that weak acid leaching, such as a combination of dilute acetic acid and partial dissolution, is crucial to limit the contribution from non-carbonate phases (Zhang et al., 2015; Tostevin et al., 2016a; Verdel et al., 2018; Cao et al., 2020). Yet, the REE patterns of non-carbonate phases in carbonate rocks, e.g. Fe–Mn oxides and organic matter, have been surprisingly overlooked so far. Our results demonstrate that a significant proportion of the rock's total REE can be preserved in non-carbonate phases (Fig. 1), and the acetic acid leachates (i.e. fraction 2) exhibit consistently high Y/Ho ratios in both pure limestones and impure dolostones. We therefore recommend ammonium acetate pre-leaching followed by partial digestion with dilute acetic acid

as a favourable procedure for REE analysis in carbonate rocks. Nevertheless, while dilute acetic acid leaching effectively minimises non-carbonate phase contamination, it cannot ensure the extraction of pristine REE patterns (Figs. 4, 5), which is possibly more related to diagenesis (see below). In-situ microanalysis (e.g. laser ablation ICP–MS) provides a potential means of retrieving pristine REE patterns, yet its application is hindered by generally lower analytical precision and resultant erratic REE patterns compared with solution ICP-MS (e.g. Wyndham et al., 2004; Li et al., 2019).

The demonstrable carbonate REE patterns reflect the fluid characteristics from which they precipitate and fractionation processes during and/or after deposition. It is frequently mentioned in the literature that carbonate-bound REE are resistant to diagenesis, and this has been confirmed at least for some pure carbonate rocks (Webb et al., 2009; Hood et al., 2018; Liu et al., 2019), though mobilization of REE in carbonate rocks during diagenesis has also been recognized (e.g. Webb et al., 2009). The commonly invoked evidence in support of this resistance includes assumptions that the diagenetic fluid is depleted in REE and/or has similar REE patterns to seawater (e.g. Banner et al., 1988). However, modern porewaters have non-seawater-like REE patterns and several orders of magnitude higher REE concentrations compared to seawater, which can potentially alter carbonate REE patterns. For example, Skinner et al. (2019) has illustrated the overprinting of foraminiferal REE patterns toward LREE/MREE enrichment by porewaters during early diagenesis. In this regard, recent REE studies on marine carbonate rocks with improved leaching methods reveal that non-seawater-like REE patterns are surprisingly common, for example, during negative carbon isotope excursions of the Neoproterozoic Era (e.g. Ward et al., 2019; Zhao et al., 2021), posing a challenge to our understanding of REE diagenetic behaviour.

Our phase partitioning experiments and modelling results demonstrate that carbonate REE patterns are sensitive to surrounding fluid characteristics and can be modified at a relatively low fluid/rock ratio in the presence of early diagenetic porewaters. Importantly, most Precambrian carbonate sediments formed at or below the sediment-water interface (Cantine et al., 2020), as carbonate minerals precipitating and/or later recrystallizing in conditions dominated by porewater chemistry. It is thus unsurprising that non-seawater-like REE patterns are common in Precambrian carbonate rocks (Fig. 13). It should be stressed that although our results suggest that REE are mobile during early diagenetic (syndepositional) processes, it does not necessarily mean that other proxies have been mobilized or altered as well. As shown in Taishir limestones, the preservation of primary carbon and strontium isotope ratios with non-seawater-like REE patterns suggests that proxies exhibit variable sensitivities to early diagenetic processes (Section 4.4). Similarly, non-seawater-like REE patterns observed during negative carbon isotope excursions need not be indicative of carbon isotope alteration. Moreover, although the potential influence of non-carbonate phase dissolution (e.g. Fe–Mn oxide) on other isotopic systems remains unclear at this stage, the globally correlative nature of sulfur and uranium isotopes in Member III of the Doushantuo Formation (Shuram anomaly) implies that they might not be altered significantly (Zhang et al., 2019; Shi et al., 2022; Dodd et al., 2023).

Our modelling results also indicate that carbonate Ce anomalies are affected by pore fluids (Fig. 14) and hence may not be primary seawater values, but instead reflect porewaters or a combination of both. The elevated REE concentration combined with an aberrant pattern would be the key to determining the fidelity of REE data and thus Ce anomaly. Indiscriminate use of Ce anomalies with non-seawater-like REE patterns should be avoided because these REE patterns could also reflect unusual characteristics of local seawater (e.g. in some restricted environments) and/or diagenetic effects. During early diagenetic processes, the shallow porewater REE concentrations and patterns are controlled by the particulate flux of REE carrier phases. A greater flux to the seafloor and subsequent dissolution and/or decomposition at the sediment-water interface leads to elevated porewater REE concentrations, overprinting the original sediment REE patterns (Fig. 13). As such, impure carbonate (e.g. detritus-rich) and/or originally organic-rich sediments would appear to bear a greater risk of being affected by non-carbonate phase dissolution before lithification. Conversely, early diagenesis could also impart seawater REE characteristics to detritus-rich sedimentary rocks. For instance, siliceous shales of the Doushantuo Formation Miaohe Member (Member IV) were deposited under anoxic conditions (Bridger et al., 2021), but exhibit seawater-like REE patterns with negative Ce anomalies that are interpreted to reflect early diagenetic exchange with REE carrier phases (silica and organic matter), transported to the seafloor during deposition (Zhang and Shields, 2022). Therefore, early diagenetic exchange with diverse REE-carrier phases needs to be taken into account when interpreting REE patterns, and any non-seawater-like REE patterns in carbonate rocks need to be viewed with caution before their Ce anomalies or other features can be used to interpret paleoseawater chemistry.

5. Conclusions

We have applied a sequential leaching scheme to extract different REE-bearing phases in carbonate rocks. The results indicate that the exchangeable phase comprises a negligible proportion of measured REE, although it is an important host phase for elements such as Sr, Ba and K. The non-carbonate phases, including phosphates, Fe–Mn oxides, organic matter and silicates, can make up more than 50% of the overall REE content of carbonate rocks. While the acidified hydroxylamine hydrochloride is effective in dissolving Fe–Mn oxides, it can also dissolve phosphate minerals, and any remaining dolomite. Thus, the dominantly MREE-enriched patterns in the 'Fe–Mn oxide' phase of GYZ dolostones instead indicate phosphate dissolution. On the other hand, the equivalent leachates of Taishir limestones bear few effects of phosphate dissolution, whereby the LREE/MREE-enriched patterns of the Fe–Mn oxide phase are attributed to hydrothermal processes and continuous exchange of oxides with marine fluids after initial precipitation. To our knowledge, there is no ideal way to separate organic matter without attacking other phases. Additional studies are therefore required to further improve REE partitioning methodology, in order to better understand the role of organic matter in the cycling of REE and metal isotopes.

In spite of gentle sequential leaching, the carbonate phase of impure dolostones from the Gaoyuzhuang Formation exhibits non-seawater-like REE patterns, which are attributed to diagenetic effects, whereas the prevalent negative Eu anomalies in the impure dolostones are here interpreted to reflect local seawater characteristics. In addition, non-seawater-like REE patterns are also observed in the carbonate phase of well-preserved Taishir limestones. Similar patterns have been reported in modern porewaters that also have several orders of magnitude higher REE concentrations than ambient seawater, highlighting considerable potential to modify carbonate REE patterns. Considering the similarity of REE patterns between the carbonate and Fe–Mn oxide fractions, these patterns are attributed to REE exchange during early diagenesis, possibly due to elevated porewater REE concentrations as a result of the particulate REE carrier flux, primarily Fe–Mn oxides and organic matter, to the seafloor. This view is supported by a simple fluid-rock interaction model, which suggests that REE can be mobilized at relatively low fluid/rock ratios in shallow marine porewaters and generally reproduces the measured carbonate REE patterns. We propose that covariation diagrams integrating REE concentrations and other REE parameters may be helpful in identifying the overprinting of a seawater REE signature. Furthermore, the mobilization of REE during early diagenesis could also explain the non-seawater-like REE patterns associated with intervals of negative $\delta^{13}C$ values, whereby carbonate REE patterns reflect dissolution of REE-enriched phases (e.g. Fe–Mn oxides), whereas carbon isotopes remained buffered by seawater DIC. Such non-seawater-like carbonate REE patterns might be expected in the Precambrian, during which often mineralogically metastable carbonate minerals formed at or

below the sediment-water interface and so likely underwent diagenetic exchange with shallow porewaters. Although how such exchange might be relevant for isotopic systems has not been specifically investigated, the co-occurrence of non-seawater-like REE patterns with primary C, Sr, S and U isotopes suggests to us that carbonate REE patterns are a poor measure of the diagenetic alteration of other geochemical proxies, which instead should be evaluated individually. Because Ce anomalies in carbonate rocks are also influenced by porewater exchange, we recommend that interpretations of local redox conditions take into account REE patterns as a whole, and where possible analyse non-carbonate phases, too.

Declaration of Competing Interest

The authors declare that they have no known competing financial interests or personal relationships that could have appeared to influence the work reported in this paper.

Data availability

All data used in the article is available in supplementary materials.

Acknowledgements

KZ acknowledges support from the China Scholarship Council and a University College London Faculty Dean's Prize. GS acknowledges financial support from NERC (NE/R010129/1). Both authors thank Gary Tarbuck for his invaluable technical support. Ying Zhou is also thanked for helpful discussions. The manuscript benefited greatly from the comments of one anonymous reviewer, and the especially constructive critique of Johan Schijf. We are also grateful to Karen H. Johannesson for her editorial handling.

Appendix A. Supplementary data

Supplementary data to this article can be found online at https://doi.org/10.1016/j.chemgeo.2023.121619.

References

Abbott, A.N., Haley, B.A., McManus, J., Reimers, C.E., 2015. The sedimentary flux of dissolved rare earth elements to the ocean. Geochim. Cosmochim. Acta 154, 186–200.
Abbott, A.N., Löhr, S., Trethewy, M., 2019. Are clay minerals the primary control on the oceanic rare earth element budget? Front. Mar. Sci. 6, 1–19.
Adebayo, S.B., Cui, M., Hong, T., White, C.D., Martin, E.E., Johannesson, K.H., 2018. Rare earth elements geochemistry and Nd isotopes in the Mississippi River and Gulf of Mexico Mixing Zone. Front. Mar. Sci. 5, 1–18.
Alibo, D.S., Nozaki, Y., 1999. Rare earth elements in seawater: particle association, shale-normalization, and Ce oxidation. Geochim. Cosmochim. Acta 63 (3–4), 363–372.
Bailey, T.R., McArthur, J.M., Prince, H., Thirlwall, M.F., 2000. Dissolution methods for strontium isotope stratigraphy: whole rock analysis. Chem. Geol. 167 (3–4), 313–319.
Banner, J.L., Hanson, G.N., 1990. Calculation of simultaneous isotopic and trace element variations during water-rock interaction with applications to carbonate diagenesis. Geochim. Cosmochim. Acta 54 (11), 3123–3137.
Banner, J.L., Hanson, G.N., Meyers, W.J., 1988. Rare earth element and Nd isotopic variations in regionally extensive dolomites from the Burlington-Keokuk Formation (Mississippian): Implications for Ree Mobility during Carbonate Diagenesis. SEPM J. Sediment. Res. 58 (11), 3123–3137.
Bau, M., 1991. Rare-earth element mobility during hydrothermal and metamorphic fluid-rock interaction and the significance of the oxidation state of europium. Chem. Geol. 93 (3–4), 219–230.
Bau, M., 1999. Scavenging of dissolved yttrium and rare earths by precipitating iron oxyhydroxide: experimental evidence for Ce oxidation, Y-Ho fractionation, and lanthanide tetrad effect. Geochim. Cosmochim. Acta 63 (1), 67–77.
Bau, M., Möller, P., 1992. Rare earth element fractionation in metamorphogenic hydrothermal calcite, magnesite and siderite. Mineral. Petrol. 45 (3–4), 231–246.
Bau, M., Möller, P., Dulski, P., 1997. Yttrium and lanthanides in eastern Mediterranean seawater and their fractionation during redox-cycling. Mar. Chem. 56 (1–2), 123–131.
Bau, M., Schmidt, K., Koschinsky, A., Hein, J., Kuhn, T., Usui, A., 2014. Discriminating between different genetic types of marine ferro-manganese crusts and nodules based on rare earth elements and yttrium. Chem. Geol. 381, 1–9.
Bayon, G., German, C.R., Boella, R.M., Milton, J.A., Taylor, R.N., Nesbitt, R.W., 2002. An improved method for extracting marine sediment fractions and its application to Sr and Nd isotopic analysis. Chem. Geol. 187 (3–4), 179–199.
Bayon, G., Birot, D., Ruffine, L., Caprais, J.C., Ponzevera, E., Bollinger, C., Donval, J.P., Charlou, J.L., Voisset, M., Grimaud, S., 2011. Evidence for intense REE scavenging at cold seeps from the Niger Delta margin. Earth Planet. Sci. Lett. 312 (3–4), 443–452.
Bayon, G., Lemaitre, N., Barrat, J.A., Wang, X., Feng, D., Duperron, S., 2020a. Microbial utilization of rare earth elements at cold seeps related to aerobic methane oxidation. Chem. Geol. 555, 119832.
Bayon, G., Douglas, G.B., Denton, G.J., Monin, L., De Deckker, P., 2020b. Preferential Riverine export of fine volcanogenic particles to the Southeast Australian margin. Front. Mar. Sci. 7, 89.
Bellefroid, E.J., Hood, A.V.S., Hoffman, P.F., Thomas, M.D., Reinhard, C.T., Planavsky, N.J., 2018. Constraints on Paleoproterozoic atmospheric oxygen levels. Proc. Natl. Acad. Sci. 115 (32), 8104–8109.
Bjerrum, C.J., Canfield, D.E., 2011. Towards a quantitative understanding of the late Neoproterozoic carbon cycle. Proc. Natl. Acad. Sci. U. S. A. 108 (14), 5542–5547.
Bold, U., Smith, E.F., Rooney, A.D., Bowring, S.A., Buchwaldt, R., Dudás, F.O., Ramezani, J., Crowley, J.L., Schrag, D.P., Macdonald, F.A., 2016. Neoproterozoic stratigraphy of the zavkhan terrane of Mongolia: the backbone for cryogenian and early ediacaran chemostratigraphic records. Am. J. Sci. 315 (11), 1–63.
Bolhar, R., Hofmann, A., Siahi, M., Feng, Y.X., Delvigne, C., 2015. A trace element and Pb isotopic investigation into the provenance and deposition of stromatolitic carbonates, ironstones and associated shales of the ~3.0Ga Pongola Supergroup, Kaapvaal Craton. Geochim. Cosmochim. Acta 158, 57–78.
Brand, U., Veizer, J., 1980. Chemical Diagenesis of a Multicomponent Carbonate System–1: Trace elements. SEPM J. Sediment. Res. 50 (3), 987–998.
Bridger, P., Poulton, S.W., Zhou, Y., Li, C., Zhang, K., Shields, G.A., 2021. The Ediacaran 'Miaohe Member' of South China: new insights from palaeoredox proxies and stable isotope data. Geol. Mag. 1–15.
Bridgestock, L., Te Hsieh, Y., Porcelli, D., Homoky, W.B., Bryan, A., Henderson, G.M., 2018. Controls on the barium isotope compositions of marine sediments. Earth Planet. Sci. Lett. 481, 101–110.
Byrne, R.H., Kim, K.H., 1990. Rare earth element scavenging in seawater. Geochim. Cosmochim. Acta 54 (10), 2645–2656.
Byrne, R.H., Li, B., 1995. Comparative complexation behavior of the rare earths. Geochim. Cosmochim. Acta 59 (22), 4575–4589.
Byrne, R.H., Liu, X., 1998. A coupled riverine-marine fractionation model for dissolved rare earths and yttrium. Aquat. Geochem. 4 (1), 103–121.
Canfield, D.E., Knoll, A.H., Poulton, S.W., Narbonne, G.M., Dunning, G.R., 2020. Carbon isotopes in clastic rocks and the neoproterozoic carbon cycle. Am. J. Sci. 320 (2), 97–124.
Cantine, M.D., Knoll, A.H., Bergmann, K.D., 2020. Carbonates before skeletons: A database approach. Earth-Sci. Rev. 201, 103065.
Cao, C., Liu, X.-M., Bataille, C.P., Liu, C., 2020. What do Ce anomalies in marine carbonates really mean? A perspective from leaching experiments. Chem. Geol. 532, 119413.
Chassé, M., Griffin, W.L., O'Reilly, S.Y., Calas, G., 2019. Australian laterites reveal mechanisms governing scandium dynamics in the critical zone. Geochim. Cosmochim. Acta 260, 292–310.
Chen, X., Romaniello, S.J., Herrmann, A.D., Hardisty, D., Gill, B.C., Anbar, A.D., 2018. Diagenetic effects on uranium isotope fractionation in carbonate sediments from the Bahamas. Geochim. Cosmochim. Acta 237, 294–311.
Chester, R., Hughes, M.J., 1967. A chemical technique for the separation of ferro-manganese minerals, carbonate minerals and adsorbed trace elements from pelagic sediments. Chem. Geol. 2, 249–262.
Chou, L., Garrels, R.M., Wollast, R., 1989. Comparative study of the kinetics and mechanisms of dissolution of carbonate minerals. Chem. Geol. 78 (3–4), 269–282.
Clarkson, M.O., Müsing, K., Andersen, M.B., Vance, D., 2020. Examining pelagic carbonate-rich sediments as an archive for authigenic uranium and molybdenum isotopes using reductive cleaning and leaching experiments. Chem. Geol. 539, 119412.
Connelly, N.G., Damhus, T., Hartshorn, R.M., Hutton, A.T., 2005. Nomenclature of Inorganic Chemistry: IUPAC Recommendations 2005. The Royal Society of Chemistry.
Corkeron, M., Webb, G.E., Moulds, J., Grey, K., 2012. Discriminating stromatolite formation modes using rare earth element geochemistry: Trapping and binding versus in situ precipitation of stromatolites from the Neoproterozoic Bitter Springs Formation, Northern Territory, Australia. Precambrian Res. 212–213, 194–206.
Cui, H., Kaufman, A.J., Xiao, S., Zhu, M., Zhou, C., Liu, X.M., 2015. Redox architecture of an Ediacaran Ocean margin: Integrated chemostratigraphic (δ13C-δ34S-87Sr/86Sr-Ce/Ce*) correlation of the Doushantuo Formation, South China. Chem. Geol. 405, 48–62.
Cui, H., Kaufman, A.J., Xiao, S., Zhou, C., Liu, X.M., 2017. Was the Ediacaran Shuram Excursion a globally synchronized early diagenetic event? Insights from methane-derived authigenic carbonates in the uppermost Doushantuo Formation, South China. Chem. Geol. 450, 59–80.
Cui, H., Kitajima, K., Orland, I.J., Xiao, S., Baele, J.M., Kaufman, A.J., Denny, A., Zhou, C., Spicuzza, M.J., Fournelle, J.H., Valley, J.W., 2021. Deposition or diagenesis? Probing the Ediacaran Shuram excursion in South China by SIMS. Glob. Planet. Chang. 206, 103591.
De Baar, H.J.W., Bacon, M.P., Brewer, P.G., Bruland, K.W., 1985. Rare earth elements in the Pacific and Atlantic Oceans. Geochim. Cosmochim. Acta 49 (9), 1943–1959.
De Baar, H.J.W., German, C.R., Elderfield, H., van Gaans, P., 1988. Rare earth element distributions in anoxic waters of the Cariaco Trench. Geochim. Cosmochim. Acta 52 (5), 1203–1219.

Deng, Y., Ren, J., Guo, Q., Cao, J., Wang, H., Liu, C., 2017. Rare earth element geochemistry characteristics of seawater and porewater from deep sea in western Pacific. Sci. Rep. 7 (1), 1–13.
Deng, Y., Guo, Q., Liu, C., He, G., Cao, J., Liao, J., Liu, C., Wang, H., Zhou, J., Liu, Y., Wang, F., Zhao, B., Wei, R., Zhu, J., Qiu, H., 2022. Early diagenetic control on the enrichment and fractionation of rare earth elements in deep-sea sediments. Sci. Adv. 8 (25).
Derry, L.A., 2010. A burial diagenesis origin for the Ediacaran Shuram-Wonoka carbon isotope anomaly. Earth Planet. Sci. Lett. 294 (1–2), 152–162.
Dodd, M.S., Shi, W., Li, C., Zhang, Z., Cheng, M., Gu, H., Hardisty, D.S., Loyd, S.J., Wallace, M.W.V.S., Hood, A., Lamothe, K., Mills, B.J.W., Poulton, S.W., Lyons, T.W., 2023. Uncovering the Ediacaran Phosphorus Cycle. Nature 618 (7967), 974–980.
Dubinin, A.V., Strekopytov, S.V., 2001. Behavior of rare earth elements during leaching of the oceanic sediments. Geochem. Int. 39 (7), 692–701.
Dulski, P., 1994. Interferences of oxide, hydroxide and chloride analyte species in the determination of rare earth elements in geological samples by inductively coupled plasma-mass spectrometry. Fresenius J. Anal. Chem. 350 (4–5), 194–203.
Eberli, G.P., Swart, P.K., McNeill, D.F., Kenter, J.A.M., Anselmetti, F.S., Melim, L.A., Ginsburg, R.N., 1997. A Synopsis of the Bahamas Drilling Project: results from two Deep Core Borings Drilled on the Great Bahama Bank. Proc. Ocean Drill. Program. Initial Reports. 166, 23–41.
Elderfield, H., 1988. The Oceanic Chemistry of the Rare-Earth elements. Philos. Trans. R. Soc. A Math. Phys. Eng. Sci. 325 (1583), 105–126.
Elderfield, H., Greaves, M., 1982. The rare earth elements in seawater. Nature 296, 214–219.
Elderfield, H., Sholkovitz, E.R., 1987. Rare earth elements in the pore waters of reducing nearshore sediments. Earth Planet. Sci. Lett. 82 (3–4), 280–288.
Elderfield, H., Upstill-Goddard, R., Sholkovitz, E.R., 1990. The rare earth elements in rivers, estuaries, and coastal seas and their significance to the composition of ocean waters. Geochim. Cosmochim. Acta 54 (4), 971–991.
Emsbo, P., McLaughlin, P.I., Breit, G.N., du Bray, E.A., Koenig, A.E., 2015. Rare earth elements in sedimentary phosphate deposits: solution to the global REE crisis? Gondwana Res. 27 (2), 776–785.
Fang, H., Tang, D., Shi, X., Lechte, M., Shang, M., Zhou, X., Yu, W., 2020. Manganese-rich deposits in the Mesoproterozoic Gaoyuzhuang Formation (ca. 1.58 Ga), North China Platform: Genesis and paleoenvironmental implications. Palaeogeogr. Palaeoclimatol. Palaeoecol. 559, 109966.
Filgueiras, A.V., Lavilla, I., Bendicho, C., 2002. Chemical sequential extraction for metal partitioning in environmental solid samples. J. Environ. Monit. 4 (6), 823–857.
Freslon, N., Bayon, G., Toucanne, S., Bermell, S., Bollinger, C., Chéron, S., Etoubleau, J., Germain, Y., Khripounoff, A., Ponzevera, E., Rouget, M.-L., 2014. Rare earth elements and neodymium isotopes in sedimentary organic matter. Geochim. Cosmochim. Acta 140, 177–198.
Frimmel, H.E., 2009. Trace element distribution in Neoproterozoic carbonates as palaeoenvironmental indicator. Chem. Geol. 258 (3–4), 338–353.
Frimmel, H.E., 2010. On the reliability of stable carbon isotopes for Neoproterozoic chemostratigraphic correlation. Precambrian Res. 182 (4), 239–253.
German, R., Elderfield, H., 1990. Application of the Ce anomaly as a paleoredox indicator: the ground rules. Paleoceanogr. 5 (5), 823–833.
Gong, Q., Li, F., Lu, C., Wang, H., Tang, H., 2021. Tracing seawater- and terrestrial-sourced REE signatures in detritally contaminated, diagenetically altered carbonate rocks. Chem. Geol. 570, 120169.
Grotzinger, J.P., James, N.P., 2000. Precambrian Carbonates: Evolution of Understanding. In: J.P. Grotzinger, N.P. James (Eds.), Carbonate Sedimentation and Diagenesis in the Evolving Precambrian World, SEPM Special Publication, 67 (2000), 3-20.
Gutjahr, M., Frank, M., Stirling, C.H., Klemm, V., van de Flierdt, T., Halliday, A.N., 2007. Reliable extraction of a Deepwater trace metal isotope signal from Fe-Mn oxyhydroxide coatings of marine sediments. Chem. Geol. 242 (3–4), 351–370.
Haines, P.W., 1988. Storm-dominated mixed carbonate / siliciclastic shelf sequence displaying cycles of hummocky cross-stratification, late Proterozoic Wonoka Formation, South Australia. Sediment. Geol. 58 (2–4), 237–254.
Haley, B.A., Klinkhammer, G.P., McManus, J., 2004. Rare earth elements in pore waters of marine sediments. Geochim. Cosmochim. Acta 68 (6), 1265–1279.
Halverson, G., Porter, S., Shields, G., 2020. The Tonian and Cryogenian periods. Geol. Time Scale 2020, 495–519.
Hannigan, R.E., Sholkovitz, E.R., 2001. The development of middle rare earth element enrichments in freshwaters: Weathering of phosphate minerals. Chem. Geol. 175 (3–4), 495–508.
Hanson, G.N., 1980. Rare Earth elements in Petrogenetic Studies of Igneous Systems. Annu. Rev. Earth Planet. Sci. 8 (1), 371–406.
Hardie, L.A., 2003. Secular variations in Precambrian seawater chemistry and the timing of Precambrian aragonite seas and calcite seas. Geology 31 (9), 785–788.
Hayakawa, T., Kikui, F., Ikeda, S., 1982. The determination of I, P, B, S, as and Sn by inductively coupled plasma emission spectroscopy using lines at vacuum ultra-violet wavelengths. Spectrochim. Acta Part B At. Spectrosc. 37 (12), 1069–1073.
Higgins, J.A., Fischer, W.W., Schrag, D.P., 2009. Oxygenation of the ocean and sediments: Consequences for the seafloor carbonate factory. Earth Planet. Sci. Lett. 284 (1–2), 25–33.
Hill, A.C., Walter, M.R., 2000. Mid-Neoproterozoic (~830-750 Ma) isotope stratigraphy of Australia and global correlation. Precambrian Res. 100, 181–211.
Himmler, T., Bach, W., Bohrmann, G., Peckmann, J., 2010. Rare earth elements in authigenic methane-seep carbonates as tracers for fluid composition during early diagenesis. Chem. Geol. 277 (1–2), 126–136.
Himmler, T., Haley, B.A., Torres, M.E., Klinkhammer, G.P., Bohrmann, G., Peckmann, J., 2013. Rare earth element geochemistry in cold-seep pore waters of Hydrate Ridge, Northeast Pacific Ocean. Geo-Marine Lett. 33 (5), 369–379.
Hodgskiss, M.S.W., Lalonde, S.V., Crockford, P.W., Hutchings, A.M., 2021. A carbonate molybdenum isotope and cerium anomaly record across the end-GOE: local records of global oxygenation. Geochim. Cosmochim. Acta 313, 313–339.
Hood, A.V.S., Planavsky, N.J., Wallace, M.W., Wang, X., 2018. The effects of diagenesis on geochemical paleoredox proxies in sedimentary carbonates. Geochim. Cosmochim. Acta 232, 265–287.
Hood, A.V.S., Wallace, M.W., 2012. Synsedimentary diagenesis in a Cryogenian reef complex: Ubiquitous marine dolomite precipitation. Sediment. Geol. 255–256, 56–71.
Hood, A.V.S., Wallace, M.W., 2015. Extreme Ocean anoxia during the late Cryogenian recorded in reefal carbonates of Southern Australia. Precambrian Res. 261, 96–111.
Jiang, G., Shi, X., Zhang, S., Wang, Y., Xiao, S., 2011. Stratigraphy and paleogeography of the Ediacaran Doushantuo Formation (ca. 635-551Ma) in South China. Gondwana Res. 19 (4), 831–849.
Johannesson, K.H., Zhou, X., 1999. Origin of middle rare earth element enrichments in acid waters of a Canadian High Arctic lake. Geochim. Cosmochim. Acta 63 (1), 153–165.
Johannesson, K.H., Lyons, W.B., Bird, D.A., 1994. Rare earth element concentrations and speciation in alkaline lakes from the western U.S.A. Geophys. Res. Lett. 21 (9), 773–776.
Johnston, D.T., MacDonald, F.A., Gill, B.C., Hoffman, P.F., Schrag, D.P., 2012. Uncovering the neoproterozoic carbon cycle. Nature 483 (7389), 320–323.
Kamber, B.S., Webb, G.E., 2001. The geochemistry of late Archaean microbial carbonate: Implications for ocean chemistry and continental erosion history. Geochim. Cosmochim. Acta 65 (15), 2509–2525.
Kamber, B.S., Bolhar, R., Webb, G.E., 2004. Geochemistry of late Archaean stromatolites from Zimbabwe: evidence for microbial life in restricted epicontinental seas. Precambrian Res. 132 (4), 379–399.
Kato, Y., Yamaguchi, K.E., Ohmoto, H., 2006. Rare earth elements in Precambrian banded iron formations: Secular changes of Ce and Eu anomalies and evolution of atmospheric oxygen. In: Evolution of Early Earth's Atmosphere, Hydrosphere, and Biosphere - Constraints from Ore Deposits, 198. Geological Society of America, pp. 269–289.
Kheboian, C., Bauer, C.F., 1987. Accuracy of Selective Extraction Procedures for Metal Speciation in Model Aquatic Sediments. Anal. Chem. 59 (10), 1417–1423.
Kim, N.D., Fergusson, J.E., 1991. Effectiveness of a commonly used sequential extraction technique in determining the speciation of cadmium in soils. Sci. Total Environ. 105 (C), 191–209.
Kim, J.H., Torres, M.E., Haley, B.A., Kastner, M., Pohlman, J.W., Riedel, M., Lee, Y.J., 2012. The effect of diagenesis and fluid migration on rare earth element distribution in pore fluids of the northern Cascadia accretionary margin. Chem. Geol. 291, 152–165.
Kim, I., Kim, G., Choy, E.J., 2015. The significant inputs of trace elements and rare earth elements from melting glaciers in Antarctic coastal waters. Polar Res 34 (1), 24289.
Knoll, A.H., Hayes, J.M., Kaufman, A.J., Swett, K., Lambert, I.B., 1986. Secular variation in carbon isotope ratios from Upper Proterozoic successions of Svalbard and East Greenland. Nature 321 (6073), 832–838.
Koeppenkastrop, D., De Carlo, E.H., 1992. Sorption of rare-earth elements from seawater onto synthetic mineral particles: an experimental approach. Chem. Geol. 95 (3–4), 251–263.
Köhler, S.J., Bosbach, D., Oelkers, E.H., 2005. Do clay mineral dissolution rates reach steady state? Geochim. Cosmochim. Acta 69 (8), 1997–2006.
Land, M., Öhlander, B., Ingri, J., Thunberg, J., 1999. Solid speciation and fractionation of rare earth elements in a spodosol profile from northern Sweden as revealed by sequential extraction. Chem. Geol. 160 (1–2), 121–138.
Lau, K.V., Hardisty, D.S., 2022. Modeling the impacts of diagenesis on carbonate paleoredox proxies. Geochim. Cosmochim. Acta 337, 123–139.
Lawrence, M.G., Kamber, B.S., 2006. The behaviour of the rare earth elements during estuarine mixing-revisited. Mar. Chem. 100 (1–2), 147–161.
Lawrence, M.G., Greig, A., Collerson, K.D., Kamber, B.S., 2006. Rare Earth Element and Yttrium Variability in South East Queensland Waterways. Aquat. Geochem. 12 (1), 39–72.
Lécuyer, C., Reynard, B., Grandjean, P., 2004. Rare earth element evolution of Phanerozoic seawater recorded in biogenic apatites. Chem. Geol. 204 (1–2), 63–102.
Leybourne, M.I., Johannesson, K.H., 2008. Rare earth elements (REE) and yttrium in stream waters, stream sediments, and Fe-Mn oxyhydroxides: Fractionation, speciation, and controls over REE + Y patterns in the surface environment. Geochim. Cosmochim. Acta 72 (24), 5962–5983.
Li, D., Shields-Zhou, G.A., Ling, H.F., Thirlwall, M., 2011. Dissolution methods for strontium isotope stratigraphy: guidelines for the use of bulk carbonate and phosphorite rocks. Chem. Geol. 290 (3–4), 133–144.
Li, F., Webb, G.E., Algeo, T.J., Kershaw, S., Lu, C., Oehlert, A.M., Gong, Q., Pourmand, A., Tan, X., 2019. Modern carbonate ooids preserve ambient aqueous REE signatures. Chem. Geol. 509, 163–177.
Liao, J., Chen, J., Sun, X., Wu, Z., Deng, Y., Shi, X., Wang, Y., Chen, Y., Koschinsky, A., 2022. Quantifying the controlling mineral phases of rare-earth elements in deep-sea pelagic sediments. Chem. Geol. 595, 120792.
Lin, Y.-B., Wei, H.-Z., Jiang, S.-Y., Hohl, S., Lei, H.-L., Liu, X., Dong, G., 2020. Accurate Determination of Barium Isotopic Compositions in Sequentially Leached Phases from Carbonates by double Spike-thermal Ionization Mass Spectrometry (DS-TIMS). Anal. Chem. 92 (3), 2417–2424.
Ling, H.-F., Chen, X., Li, D., Wang, D., Shields-Zhou, G.A., Zhu, M., 2013. Cerium anomaly variations in Ediacaran–earliest Cambrian carbonates from the Yangtze

Gorges area, South China: implications for oxygenation of coeval shallow seawater. Precambrian Res. 225, 110–127.
Liu, X.-M., Hardisty, D.S., Lyons, T.W., Swart, P.K., 2019. Evaluating the fidelity of the cerium paleoredox tracer during variable carbonate diagenesis on the Great Bahamas Bank. Geochim. Cosmochim. Acta 248, 25–42.
Liu, X.M., Kah, L.C., Knoll, A.H., Cui, H., Wang, C., Bekker, A., Hazen, R.M., 2021. A persistently low level of atmospheric oxygen in Earth's middle age. Nat. Commun. 12 (1), 1–7.
MacRae, N.D., Nesbitt, H.W., Kronberg, B.I., 1992. Development of a positive Eu anomaly during diagenesis. Earth Planet. Sci. Lett. 109 (3–4), 585–591.
Mclennan, S.M., 1989. Rare earth elements in sedimentary rocks: influence of provenance and Sedimentary Processes. Rev. Mineral. Geochem. 21 (1), 169–200.
Merschel, G., Bau, M., Dantas, E.L., 2017. Contrasting impact of organic and inorganic nanoparticles and colloids on the behavior of particle-reactive elements in tropical estuaries: an experimental study. Geochim. Cosmochim. Acta 197, 1–13.
Meyer, A.C.S., Grundle, D., Cullen, J.T., 2021. Selective uptake of rare earth elements in marine systems as an indicator of and control on aerobic bacterial methanotrophy. Earth Planet. Sci. Lett. 558, 116756.
Michard, A., Albarède, F., 1986. The REE content of some hydrothermal fluids. Chem. Geol. 55 (1–2), 51–60.
Mittermüller, M., Saatz, J., Daus, B., 2016. A sequential extraction procedure to evaluate the mobilization behavior of rare earth elements in soils and tailings materials. Chemosphere 147, 155–162.
Moldoveanu, G.A., Papangelakis, V.G., 2012. Recovery of rare earth elements adsorbed on clay minerals: I. Desorption mechanism. Hydrometallurgy 117–118, 71–78.
Moldoveanu, G.A., Papangelakis, V.G., 2016. An overview of rare-earth recovery by ion-exchange leaching from ion-adsorption clays of various origins. Mineral. Mag. 80 (1), 63–76.
Möller, P., Bau, M., 1993. Rare-earth patterns with positive cerium anomaly in alkaline waters from Lake Van, Turkey. Earth Planet. Sci. Lett. 117 (3–4), 671–676.
Morse, J.W., Arvidson, R.S., Lüttge, A., 2007. Calcium carbonate formation and dissolution. Chem. Rev. 107 (2), 342–381.
Nothdurft, L.D., Webb, G.E., Kamber, B.S., 2004. Rare earth element geochemistry of late Devonian reefal carbonates, Canning Basin, Western Australia: confirmation of a seawater REE proxy in ancient limestones. Geochim. Cosmochim. Acta 68 (2), 263–283.
Nozaki, Y., Zhang, J., Amakawa, H., 1997. The fractionation between Y and Ho in the marine environment. Earth Planet. Sci. Lett. 148 (1–2), 329–340.
O'Connell, B., Wallace, M.W., Hood, A.V.S., Lechte, M.A., Planavsky, N.J., 2020. Iron-rich carbonate tidal deposits, Angepena Formation, South Australia: A redox-stratified Cryogenian basin. Precambrian Res. 342, 105668.
Ohta, A., Kawabe, I., 2001. REE(III) adsorption onto Mn dioxide (δ-MnO2) and Fe oxyhydroxide: Ce(III) oxidation by δ-MnO2. Geochim. Cosmochim. Acta 65 (5), 695–703.
Oonk, P.B.H., Mason, P.R.D., Tsikos, H., Bau, M., 2018. Fraction-specific rare earth elements enable the reconstruction of primary seawater signatures from iron formations. Geochim. Cosmochim. Acta 238, 102–122.
Palmer, M.R., 1985. Rare earth elements in foraminifera tests. Earth Planet. Sci. Lett. 73, 285–298.
Paul, S.A.L., Volz, J.B., Bau, M., Köster, M., Kasten, S., Koschinsky, A., 2019. Calcium phosphate control of REY patterns of siliceous-ooze-rich deep-sea sediments from the central equatorial Pacific. Geochim. Cosmochim. Acta 251, 56–72.
Phan, T.T., Hakala, J.A., Lopano, C.L., Sharma, S., 2019. Rare earth elements and radiogenic strontium isotopes in carbonate minerals reveal diagenetic influence in shales and limestones in the Appalachian Basin. Chem. Geol. 509, 194–212.
Picone, N., Op den Camp, H.J., 2019. Role of rare earth elements in methanol oxidation. Curr. Opin. Chem. Biol. 49, 39–44.
Piper, D.Z., Wandless, G.A., 1992. Hydroxylamine Hydrochloride-Acetic Acid-Soluble and -Insoluble Fractions of Pelagic Sediment: Readsorption Revisited. Environ. Sci. Technol. 26 (12), 2489–2493.
Planavsky, N., Bekker, A., Rouxel, O.J., Kamber, B., Hofmann, A., Knudsen, A., Lyons, T. W., 2010. Rare Earth Element and yttrium compositions of Archean and Paleoproterozoic Fe formations revisited: New perspectives on the significance and mechanisms of deposition. Geochim. Cosmochim. Acta 74 (22), 6387–6405.
Poulton, S.W., Canfield, D.E., 2005. Development of a sequential extraction procedure for iron: Implications for iron partitioning in continentally derived particulates. Chem. Geol. 214 (3–4), 209–221.
Poulton, S.W., Canfield, D.E., 2006. Co-diagenesis of iron and phosphorus in hydrothermal sediments from the southern East Pacific Rise: Implications for the evaluation of paleoseawater phosphate concentrations. Geochim. Cosmochim. Acta 70 (23), 5883–5898.
Pourret, O., Davranche, M., Gruau, G., Dia, A., 2007. Rare earth elements complexation with humic acid. Chem. Geol. 243 (1–2), 128–141.
Quinn, K.A., Byrne, R.H., Schijf, J., 2006. Sorption of yttrium and rare earth elements by amorphous ferric hydroxide: Influence of solution complexation with carbonate. Geochim. Cosmochim. Acta 70 (16), 4151–4165.
Rongemaille, E., Bayon, G., Pierre, C., Bollinger, C., Chu, N.C., Fouquet, Y., Riboulot, V., Voisset, M., 2011. Rare earth elements in cold seep carbonates from the Niger delta. Chem. Geol. 286 (3–4), 196–206.
Rooney, A.D., Macdonald, F.A., Strauss, J.V., Dudás, F.Ö., Hallmann, C., Selby, D., 2014. Re-Os geochronology and coupled Os-Sr isotope constraints on the Sturtian snowball Earth. Proc. Natl. Acad. Sci. U. S. A. 111 (1), 51–56.
Rose, C.V., Swanson-Hysell, N.L., Husson, J.M., Poppick, L.N., Cottle, J.M., Schoene, B., Maloof, A.C., 2012. Constraints on the origin and relative timing of the Trezona δ 13C anomaly below the end-Cryogenian glaciation. Earth Planet. Sci. Lett. 319–320, 241–250.
Rothman, D.H., Hayes, J.M., Summons, R.E., 2003. Dynamics of the Neoproterozoic carbon cycle. Proc. Natl. Acad. Sci. U. S. A. 100 (14), 8124–8129.
Rudolph, W.W., Irmer, G., 2015. Hydration and ion pair formation in aqueous Y3+-salt solutions. Dalton Trans. 44 (42), 18492–18505.
Sandberg, P.A., 1983. An oscillating trend in Phanerozoic non-skeletal carbonate mineralogy. Nature 305 (5929), 19–22.
Sawaki, Y., Ohno, T., Tahata, M., Komiya, T., Hirata, T., Maruyama, S., Windley, B.F., Han, J., Shu, D., Li, Y., 2010. The Ediacaran radiogenic Sr isotope excursion in the Doushantuo Formation in the three Gorges area, South China. Precambrian Res. 176 (1–4), 46–64.
Schijf, J., Byrne, R.H., 2021. Speciation of yttrium and the rare earth elements in seawater: Review of a 20-year analytical journey. Chem. Geol. 584, 120479.
Schijf, J., Marshall, K.S., 2011. YREE sorption on hydrous ferric oxide in 0.5M NaCl solutions: A model extension. Mar. Chem. 123 (1–4), 32–43.
Schijf, J., De Baar, H.J.W., Millero, F.J., 1995. Vertical distributions and speciation of dissolved rare earth elements in the anoxic brines of Bannock Basin, eastern Mediterranean Sea. Geochim. Cosmochim. Acta 59 (16), 3285–3299.
Schijf, J., Christenson, E.A., Byrne, R.H., 2015. YREE scavenging in seawater: A new look at an old model. Mar. Chem. 177, 460–471.
Schrag, D.P., Higgins, J.A., Macdonald, F.A., Johnston, D.T., 2013. Authigenic carbonate and the history of the global carbon cycle. Science 339 (6119), 540–543.
Shang, M., Tang, D., Shi, X., Zhou, L., Zhou, X., Song, H., Jiang, G., 2019. A pulse of oxygen increase in the early Mesoproterozoic Ocean at ca. 1.57–1.56 Ga. Earth Planet. Sci. Lett. 527, 115797.
Shannon, R.D., 1976. Revised effective ionic radii and systematic studies of interatomic distances in halides and chalcogenides. Acta. Crystallogr. Sect. A 32 (5), 751–767.
Shi, W., Mills, B.J.W., Li, C., Poulton, S.W., Krause, A.J., He, T., Zhou, Y., Cheng, M., Shields, G.A., 2022. Decoupled oxygenation of the Ediacaran Ocean and atmosphere during the rise of early animals. Earth Planet. Sci. Lett. 591, 117619.
Shields, G.A., 2002. "Molar-tooth microspar": A chemical explanation for its disappearance ~ 750 Ma. Terra Nova 14 (2), 108–113.
Shields, G.A., Mills, B.J.W., 2017. Tectonic controls on the long-term carbon isotope mass balance. Proc. Natl. Acad. Sci. U. S. A. 114 (17), 4318–4323.
Shields, G.A., Stille, P., 1998. Stratigraphic Trends in Cerium Anomaly in Authigenic Marine Carbonates and Phosphates: Diagenetic Alteration or Seawater Signals? Mineral. Mag. 62A (3), 1387–1388.
Shields, G., Stille, P., 2001. Diagenetic constraints on the use of cerium anomalies as palaeoseawater redox proxies: an isotopic and REE study of Cambrian phosphorites. Chem. Geol. 175 (1–2), 29–48.
Shields, G., Stille, P., Brasier, M.D., Atudorei, N., 1997. Stratified oceans and oxygenation of the late Precambrian environment: a post glacial geochemical record from the Neoproterozoic of W. Mongolia. Terra Nova 9 (3–6), 218–222.
Shields, G.A., Brasier, M.D., Stille, P., Dorjnamjaa, D., 2002. Factors contributing to high δ13C values in Cryogenian limestones of western Mongolia. Earth Planet. Sci. Lett. 196 (3–4), 99–111.
Shields, G.A., Mills, B.J.W., Zhu, M., Raub, T.D., Daines, S.J., Lenton, T.M., 2019. Unique Neoproterozoic carbon isotope excursions sustained by coupled evaporite dissolution and pyrite burial. Nat. Geosci. 12 (10), 823–827.
Sholkovitz, E.R., 1989. Artifacts associated with the chemical leaching of sediments for rare-earth elements. Chem. Geol. 77 (1), 47–51.
Sholkovitz, E.R., 1993. The geochemistry of rare earth elements in the Amazon River estuary. Geochim. Cosmochim. Acta 57 (10), 2181–2190.
Sholkovitz, E.R., Landing, W.M., Lewis, B.L., 1994. Ocean particle chemistry: the fractionation of rare earth elements between suspended particles and seawater. Geochim. Cosmochim. Acta 58 (6), 1567–1579.
Skinner, L.C., Sadekov, A., Brandon, M., Greaves, M., Plancherel, Y., de la Fuente, M., Gottschalk, J., Souanef-Ureta, S., Sevilgen, D.S., Scrivner, A.E., 2019. Rare Earth elements in early-diagenetic foraminifer 'coatings': Pore-water controls and potential palaeoceanographic applications. Geochim. Cosmochim. Acta 245, 118–132.
Slack, J.F., Grenne, T., Bekker, A., Rouxel, O.J., Lindberg, P.A., 2007. Suboxic deep seawater in the late Paleoproterozoic: evidence from hematitic chert and iron formation related to seafloor-hydrothermal sulfide deposits, Central Arizona, USA. Earth Planet. Sci. Lett. 255 (1–2), 243–256.
Sverjensky, D.A., 1984. Europium redox equilibria in aqueous solution. Earth Planet. Sci. Lett. 67 (1), 70–78.
Tang, D., Shi, X., Wang, X., Jiang, G., 2016. Extremely low oxygen concentration in mid-Proterozoic shallow seawaters. Precambrian Res. 276, 145–157.
Tessier, A., Campbell, P.G.C., Bisson, M., 1979. Sequential Extraction Procedure for the Speciation of Particulate Trace Metals. Anal. Chem. 51 (7), 844–851.
Tostevin, R., Shields, G.A., Tarbuck, G.M., He, T., Clarkson, M.O., Wood, R.A., 2016a. Effective use of cerium anomalies as a redox proxy in carbonate-dominated marine settings. Chem. Geol. 438, 146–162.
Tostevin, R., Wood, R.A., Shields, G.A., Poulton, S.W., Guilbaud, R., Bowyer, F., Penny, A.M., He, T., Curtis, A., Hoffmann, K.H., Clarkson, M.O., 2016b. Low-oxygen waters limited habitable space for early animals. Nat. Commun. 7 (1), 12818.
Toyama, K., Terakado, Y., 2014. Experimental study of rare earth element partitioning between calcite and sodium chloride solution at room temperature and pressure. Geochem. J. 48 (5), 463–477.
Verdel, C., Phelps, B., Welsh, K., 2018. Rare earth element and 87Sr/86Sr step-leaching geochemistry of central Australian Neoproterozoic carbonate. Precambrian Res. 310, 229–242.
Voigt, M., Mavromatis, V., Oelkers, E.H., 2017. The experimental determination of REE partition coefficients in the water-calcite system. Chem. Geol. 462, 30–43.

Wallace, M.W., Hood, A., Shuster, A., Greig, A., Planavsky, N.J., Reed, C.P., 2017. Oxygenation history of the Neoproterozoic to early Phanerozoic and the rise of land plants. Earth Planet. Sci. Lett. 466, 12–19.
Ward, J.F., Verdel, C., Campbell, M.J., Leonard, N., Duc Nguyen, A., 2019. Rare earth element geochemistry of Australian Neoproterozoic carbonate: Constraints on the Neoproterozoic oxygenation events. Precambrian Res. 335, 105471.
Webb, G.E., Kamber, B.S., 2000. Rare earth elements in Holocene reefal microbialites: a new shallow seawater proxy. Geochim. Cosmochim. Acta 64 (9), 1557–1565.
Webb, G.E., Nothdurft, L.D., Kamber, B.S., Kloprogge, J.T., Zhao, J.X., 2009. Rare earth element geochemistry of scleractinian coral skeleton during meteoric diagenesis: A sequence through neomorphism of aragonite to calcite. Sedimentology 56 (5), 1433–1463.
Weill, D.F., Drake, M.J., 1973. Europium anomaly in plagioclase feldspar: experimental results and semiquantitative model. Science 180 (4090), 1059–1060.
Weyl, P.K., 1960. Porosity through dolomitization: conservation-of-mass requirements. SEPM J. Sediment. Res. 30 (1), 85–90.
Willis, S.S., Johannesson, K.H., 2011. Controls on the geochemistry of rare earth elements in sediments and groundwaters of the Aquia aquifer, Maryland, USA. Chem. Geol. 285 (1–4), 32–49.
Wu, Z., Guo, W., Jin, L., Hu, S., 2018. Effect of signal acquisition mode on isotope ratio precision and accuracy in ICP-quadrupole-MS analysis. Microchem. J. 142, 251–257.
Wyndham, T., McCulloch, M., Fallon, S., Alibert, C., 2004. High-resolution coral records of rare earth elements in coastal seawater: Biogeochemical cycling and a new environmental proxy. Geochim. Cosmochim. Acta 68 (9), 2067–2080.
Yang, C., Rooney, A.D., Condon, D.J., Li, X.H., Grazhdankin, D.V., Bowyer, F.T., Hu, C., Macdonald, F.A., Zhu, M., 2021. The tempo of Ediacaran evolution. Sci. Adv. 7 (45), 1–11.
Yoshioka, H., Asahara, Y., Tojo, B., Ichi Kawakami, S., 2003. Systematic variations in C, O, and Sr isotopes and elemental concentrations in neoproterozoic carbonates in Namibia: Implications for a glacial to interglacial transition. Precambrian Res. 124 (1), 69–85.
Zhai, M., Hu, B., Zhao, T., Peng, P., Meng, Q., 2015. Late Paleoproterozoic–Neoproterozoic multi-rifting events in the North China Craton and their geological significance: A study advance and review. Tectonophysics 662, 153–166.
Zhang, K., Shields, G.A., 2022. Sedimentary Ce anomalies: Secular change and implications for paleoenvironmental evolution. Earth-Sci. Rev. 229, 104015.
Zhang, K., Zhu, X., Yan, B., 2015. A refined dissolution method for rare earth element studies of bulk carbonate rocks. Chem. Geol. 412, 82–91.
Zhang, K., Zhu, X., Wood, R.A., Shi, Y., Gao, Z., Poulton, S.W., 2018. Oxygenation of the Mesoproterozoic Ocean and the evolution of complex eukaryotes. Nat. Geosci. 11 (5), 345–350.
Zhang, F., Xiao, S., Romaniello, S.J., Hardisty, D., Li, C., Melezhik, V., Pokrovsky, B., Cheng, M., Shi, W., Lenton, T.M., Anbar, A.D., 2019. Global marine redox changes drove the rise and fall of the Ediacara biota. Geobiology 17 (6), 594–610.
Zhao, Y.Y., Zheng, Y.F., Chen, F., 2009. Trace element and strontium isotope constraints on sedimentary environment of Ediacaran carbonates in southern Anhui, South China. Chem. Geol. 265 (3–4), 345–362.
Zhao, Y., Wei, W., Li, S., Yang, T., Zhang, R., Somerville, I., Santosh, M., Wei, H., Wu, J., Yang, J., Chen, W., Tang, Z., 2021. Rare earth element geochemistry of carbonates as a proxy for deep-time environmental reconstruction. Palaeogeogr. Palaeoclimatol. Palaeoecol. 574, 110443.
Zhong, S., Mucci, A., 1995. Partitioning of rare earth elements (REEs) between calcite and seawater solutions at 25°C and 1 atm, and high dissolved REE concentrations. Geochim. Cosmochim. Acta 59 (3), 443–453.
Zoll, A.M., Schijf, J., 2012. A surface complexation model of YREE sorption on Ulva lactuca in 0.05-5.0M NaCl solutions. Geochim. Cosmochim. Acta 97, 183–199.